Construction and Building Materials 123 (2016) 78–98

Contents lists available at ScienceDirect

Construction and Building Materials

journal homepage: www.elsevier.com/locate/conbuildmat

Assessment of performance of steel and GFRP bars as injected anchors in masonry walls

Francesca Ceroni [a,*], Roberto Cuzzilla [b], Marisa Pecce [b]

[a] University of Napoli 'Parthenope', Engineering Department, Centro Direzionale is. C4, 80143 Napoli, Italy
[b] University of Sannio, Engineering Department, Piazza Roma 21, 82100 Benevento, Italy

HIGHLIGHTS

- Experimental pull-out tests on steel and GFRP bars as injected anchors in masonry walls.
- Effect of bar diameter and type, grout type on the bond behaviour and strength.
- Comparison with several literature and code provisions for different failure modes.
- Parametric analysis for assessing injected anchors reliability under seismic actions.

ARTICLE INFO

Article history:
Received 1 March 2016
Received in revised form 22 June 2016
Accepted 24 June 2016
Available online 5 July 2016

Keywords:
Masonry walls
Out-of-plane mechanisms
Injected anchors
Pull-out test
Steel bars
GFRP bars
Bond behaviour
Seismic actions

ABSTRACT

The first part of the paper presents the results of two series of in situ pull-out tests of injected anchors embedded in existing yellow tuff masonry walls. Anchors are made of steel and GFRP bars with diameter of 12 and 20 mm and were embedded by means of two types of grout: a cement-based and a pozzolana-based grout. The results were examined in terms of both maximum load and displacement to determine the most efficient bar-grout coupling. The experimental pull-out forces are also compared with the predictions given by several literature formulas.

The second part of the paper is devoted to verify the efficiency of the tested injected anchor systems for avoiding out-of-plane damage mechanisms in masonry walls having varying slenderness and subjected to horizontal forces; to this aim parametric analyses were performed to calculate the seismic acceleration required to activate several out-of-plane mechanisms and to verify the effectiveness of injected anchors similar to those experimentally tested into avoiding them.

1. Introduction

The structural weakness of existing masonry constructions is related to the particular properties of the masonry materials and to the utilized design/construction approach, both of which depend on the construction period and the geographical area. The collapse mechanisms observed in masonry buildings can be generally distinguished into two categories: local and global structural failures. In particular, the structural behaviour of a masonry building strongly depends on presence and effectiveness of connections between vertical and horizontal resistant elements, i.e. walls and floors. The 'box' behaviour of a masonry building, which allows activating the in-plane flexural and shear strengths of the walls and, thus, the best performance for the building especially under horizontal actions, is generally assured if good connections (Lourenco et al., 2011 [1], Senaldi et al., 2014 [2]) between vertical walls and floors exist; good connection may, indeed, avoid the activation of out-of-plane mechanisms of the walls, i.e. a local failure (Valluzzi et al., 2014 [3]; Hamed and Rabinovitch, 2007 [4]). Moreover, the low tensile strength of the masonry, the masonry texture typology and the slenderness of walls may make the vertical elements extremely vulnerable to actions orthogonal to their plane and, thus, to out-of-plane mechanisms, as frequently observed after seismic events (Brandonisio et al., 2013 [5]; Modena et al., 2010 [6]).

Since the out-of-plane damage mechanisms are a very common problem within existing masonry buildings, several types of interventions have been widely performed in the past (Bento et al., 2005 [7]; Bhattacharya, 2014 [8]). Such interventions should strive to both reduce the risk of local damage mechanisms and improve

* Corresponding author.
E-mail addresses: francesca.ceroni@uniparthenope.it (F. Ceroni), roberto.cuzzilla@hotmail.it (R. Cuzzilla), pecce@unisannio.it (M. Pecce).

http://dx.doi.org/10.1016/j.conbuildmat.2016.06.124
0950-0618/

the global box behaviour by enhancing the ductility of the building and the energy dissipation under cyclic actions. Connections should also demonstrate good performance under service loading conditions in order to limit the deformability.

Common types of interventions for assuring a box-like behaviour are: 1) punctual elements connecting opposite walls, i.e. ties, which have been diffusely realized in the past in form of steel bars equipped with end plates or transversal bars for fixing them in the masonry and eventually apply a pre-tension force; 2) injected anchors embedded by means of grout into boreholes aimed to connect orthogonal walls; 3) improvement of connections of existing stringcourses with vertical walls or realization of new roof stringcourses, made of concrete or masonry beams. The latter intervention clearly improves various aspects concerning both the local and the global structural behaviour of masonry buildings, but it often requires dismantling the roof. By contrast, local interventions, such ties or injected anchors, can be regarded as minimally invasive and simpler to achieve. The rehabilitation of existing masonry structures requests, indeed, that not only safety requirements, but also the '*minimum impact*' requirements defined for heritage buildings (ICOMOS [9]) should be respected. It is worth to note that realization of 'injected' anchors represent a less reversible intervention technique compared with the use of 'dry' anchors, but the first appear a more effective strengthening technique for low strength, porous or cracked masonry where the consolidation produced by the grout may have a further positive effect since it enhances the mechanical behaviour of the masonry (Valluzzi et al., 2004 [10]).

Ties can represent a very effective technique for decreasing the seismic vulnerability of masonry structures, as also evidenced by observations of damage after recent earthquakes, especially in heritage buildings (Penna et al., 2013 [11]; Modena et al., 2010 [6]; Brandonisio et al., 2013 [5]). Such types of interventions have been applied in existing masonry buildings since the beginning of the 1900s in form of different types of steel bars and end-anchoring devices. More recently the use of ties made of Fibre Reinforced Plastic (FRP) materials (Ceroni and Prota, 2009 [12]) has gained attention because such materials allow realizing less invasive interventions (smaller dimensions of the ties because of the high tensile properties of FRPs and, thus, smaller holes in the masonry walls) characterized also by higher durability thanks to the inertia to corrosion phenomena, which, conversely, is often the main reason of the reduced effectiveness of the steel ties over time.

2. State of art on injected anchors

The injected anchors are usually realized by distributing the anchors at several points of weakly connected masonry walls with the aim of improving the global box-like behaviour of the whole building and avoid the partial or total out-of-plane collapse of slender masonry panels. The distribution of the connecting system along the wall height may have a further positive effect: the bending moment acting orthogonally to the plane of the wall may be reduced, since the injected anchors allow the walls behaving like a bi-dimensional plate if the dimensional ratio (height/width) of the wall is sufficiently low (approximately 1.0–1.5). By contrast, punctual connecting elements, such as ties, cannot give a similar 'plate behaviour' because they exert a boundary effects only at the base and top of each wall and, thus, the walls behave like a series of vertical beams.

Injected anchors can be effectively used for improving poor layer-to-layer connection in multi-leaf masonry walls; for such a masonry typology, also consolidation with only grout injection may represent an efficient solution for improving the mechanical properties of the whole masonry, especially in the case of poor quality mortar and large size aggregates used as filling material for the space between the two stone masonry exterior leaves (Vintzileou and Miltiadou-Fezans, 2008 [13]; Valluzzi et al., 2004 [10]).

Another application of anchors is related to the improvement of connections between structural elements and non-bearing walls in reinforced concrete framed structures (Valente et al., 2016 [14]), since the frame-infill interaction should be taken into account during the structural analysis. Because the contribution of unreinforced infill walls can be greatly compromised when submitted to reversed cyclic loading, appropriate measures should be taken in consideration to avoid brittle failure and premature disintegration of the infill walls.

Fig. 1 shows a typical lay-out of injected anchors for connecting and stiffening orthogonal masonry walls in the corners. Especially in the case of multi-leaf masonry walls, the good compatibility of the grout with the masonry is fundamental for attaining an effective connecting action between walls, reducing disaggregation of internal filling material, and avoiding weakness of corners caused by the drilling.

Low-shrinkage resin or grout are typically pressure-injected into the holes to ensure its complete filling and enhance the bond behaviour along the embedded length. Incomplete filling reduces, indeed, the bonded area of the anchor and, thus, its capacity to transfer shear stress with the consequence of reduced performance (Gigla, 2004 [16]). The low viscosity of the grout and the pressurized injection allows the grout to penetrate into the masonry texture, by filling cracks and voids surrounding the anchor. Sometimes, in cases of highly porous or extensively cracked and damaged masonry, to avoid the excessive penetration of grout into the masonry, a special flexible fabric sleeve is used to restrict the volume of the injected grout (Paganoni and D'Ayala, 2014 [17]; Algeri et al., 2010 [18]).

The anchor systems can be different (Araujo et al., 2014a [19]; Panizza et al., 2015 [20]; Algeri et al., 2010 [18]; Gigla, 2004 [16]; Tubbs et al., 2010 [21]; Fabrello-Streufert et al., 2003 [22]; Paganoni and D'Ayala, 2014 [17]), although bars, bolts, and connectors made by steel have been the most frequently used systems in the past. This means that for such type of intervention durability is a crucial aspect, especially because of corrosion phenomena, and, thus, the use of FRP bars (Benmokrane et al., 2000 [23]) may be beneficial, even if their performance under permanent loads and in harsh environmental conditions are still under investigation (Robert and Benmokrane, 2013 [24]; Ceroni et al., 2006 [25]). Furthermore, FRP materials constitute a large family, which allows for considerable flexibility in choosing the most compatible material with the masonry in terms of, for example, stiffness or thermal expansion coefficient in order to minimize the differential strain in the materials. Alternative anchoring systems fabricated using anchors spikes made of steel cords embedded in epoxy resin or in lime-based grout have also been successfully tested (Panizza et al., 2015 [20]).

The wide variety of physical and mechanical properties of all materials involved in the strengthening intervention (masonry blocks, mortar joints, anchors, grout) and the status of masonry (type of textures, degradation of mortar joints, cracking, voids, etc...) leads to highly variable performance of the anchors. The position of the bar in the grout sleeve, the surface configuration of the anchor, the grout thickness around the bar, the tensile strengths of the grout and masonry, and the presence of stresses transversal to the anchor as a result of loading conditions or grout shrinkage are other parameters that may influence the maximum pull-out force. Additionally, geometrical factors such as the spacing between adjacent anchors, the distance of the anchors from wall edges and openings, and different masonry textures can influence the maximum pull-out force. Both the overlapping of the influence areas of multiple anchors and the limitations on the influence areas

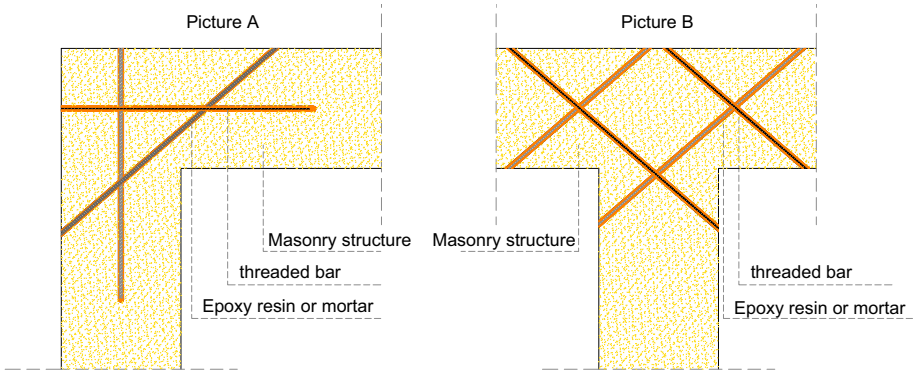

Fig. 1. a) Injected anchors for connecting walls at a corner; b) injected anchors for connecting transversal and bearing walls.

imposed by the boundary conditions may, indeed, reduce the pull-out force (MSJC, 2013 [26], ACI 318, 2011 [27]).

The maximum pull-out force depends on the bond behaviour at both the bar-grout and grout-masonry interface and the weakest failure mechanism activated. As in steel bars embedded in concrete elements (Tassios, 1979 [28]), the bond behaviour depends on adhesion, which typically is related to physical-chemical phenomena, and friction, which is related to both the bar surface and the mechanical properties of the grout and masonry, i.e. mainly the tensile strength. A further contribution is provided by the interlocking phenomena: at the bar-grout interface the interlocking depends predominantly on the surface treatment of the bar, whereas at the grout-masonry interface the interlocking depends on the ramification of the grout within the masonry.

The bond behaviour and the material strengths also influence the failure modes of injected anchors. Failure modes are usually identified as the following ones (Niker, 2012 [29]; Gigla and Wenzel, 2000 [30]; McGinley, 2006 [31]; Allen et al., 2000 [32]; Meyer and Eligehausen, 2004 [33]): 1) tensile failure of the anchor, 2) masonry failure, with the detachment of a cone-shaped surface along the anchor system, 3) bond failure at the grout-masonry interface, and 4) bond failure at the anchor system-grout interface. Tensile failure of the anchor is rarely observed because of the low tensile and shear strength of the masonry compared with the tensile strength of the anchors; it usually occurs in cases of 'long' anchors, i.e., characterized by a length-to-borehole-diameter ratio, l_e/d_b, higher than 15 (Algeri et al., 2010 [18]), or in masonry with very high mechanical properties. In general, masonry cone failure occurs in combination with sliding phenomena along the grout-masonry interface. Moreover, the mechanical properties of masonry may limit the performance of the injected anchors, even if high strength grout is used.

The maximum pull-out force depends on the failure mode activated. Some design indications are now available (Niker, 2012 [29]; Gigla and Wenzel, 2000 [30]; McGinley, 2006 [31]; Allen et al., 2000 [32]; Meyer and Eligehausen, 2004 [33]; Arifpovic and Nielsen, 2006 [34]; Cook et al., 1993 [35], MSJC, 2013 [26]; ACI 318 [27], *fib* bulletin 58 [36]) for predicting the maximum pull-out force according to the expected failure mode. Some of them were originally used for steel bars embedded in concrete elements and, then, have been applied also for predicting strength of injected anchors in masonry elements. More extensive and well-established experimental and theoretical knowledge is available regarding steel anchors embedded in concrete elements (Eligehausen and Cook, 2006 [37]; Hilti, 2011 [38], CEB, 1994 [39]; ACI 318 2011 [27]; *fib* bulletin 58, 2011 [36]).

It is worth to note that, because of the wide variety of masonry, anchors and grout types, calibration of general design formulation is not simple. Thus, experimental pull-out tests, both in real scale by means of in-situ tests or in reduced scale by means of laboratory tests, are crucial for evaluating the performances of injected anchors and assess the reliability of predicting formulations as some experimental studies have evidenced (Araujo et al., 2014a [19]; Panizza et al., 2015 [20]; Algeri et al., 2010 [18]; Gigla, 2004 [16]; Tubbs et al., 2010 [21]; Fabrello-Streufert et al., 2003 [22]; Paganoni and D'Ayala, 2014 [17]).

This paper is focussed to amply the knowledge about performance of injected anchors by means of an experimental campaign of *in-situ* pull-out tests. The results of pull-out tests on steel and glass FRP bars embedded in existing yellow tuff masonry walls using two types of injecting grout are, indeed, presented and discussed. The choice of testing the effectiveness of injected anchors is related, as previously discussed, to their higher effectiveness compared with 'dry' anchors for low strength masonry as the tuff masonry examined in this experimental program; moreover, such a masonry type has been chosen because tuff is a building material widely used for both ordinary and heritage constructions in the Southern Italy.

3. In situ pull-out tests of injected anchors in masonry wall

3.1. Description of the experimental program

Two types of deformed bars were used as anchor systems: standard steel bars and FRP bars made of glass fibres. The bars were installed in two masonry walls (Fig. 2a–c) that are part of an existing structure composed of yellow tuff blocks (with dimensions of approximately 360 mm in length, 250 mm in width and 110 mm in thickness) and lime-based mortar joints with a thickness of approximately 10 mm. Yellow tuff is a volcanic stone material consisting of consolidated ash ejected during volcanic eruptions and characterized by lapideous and pumice inclusions. It is typical of the Campania region and, more generally, of most regions of Southern and Central Italy; it has been extensively used as a construction material in the past because of its workability and both good mechanical and thermal insulation properties in relation with its low unit weight.

Both types of bars were embedded in the masonry walls using two types of premixed grout, both characterized by low shrinkage and high fluidity: a conventional cement-based grout and a *pozzolana*-based grout. '*Pozzolana*' is a fine sandy volcanic ash (Augenti and Parisi, 2000 [40]), a melted product made of piroclastite of various origins, with a variable grain size from silt to sand, which includes some gravel consisting predominantly of pumice and scoria. Pozzolana is widely available throughout the Southern Italy and it has been frequently used for realizing mortar joints in association with lime in masonry structures made of tuff or clay bricks since Roman times. Because of the similar volcanic origin, tuff can

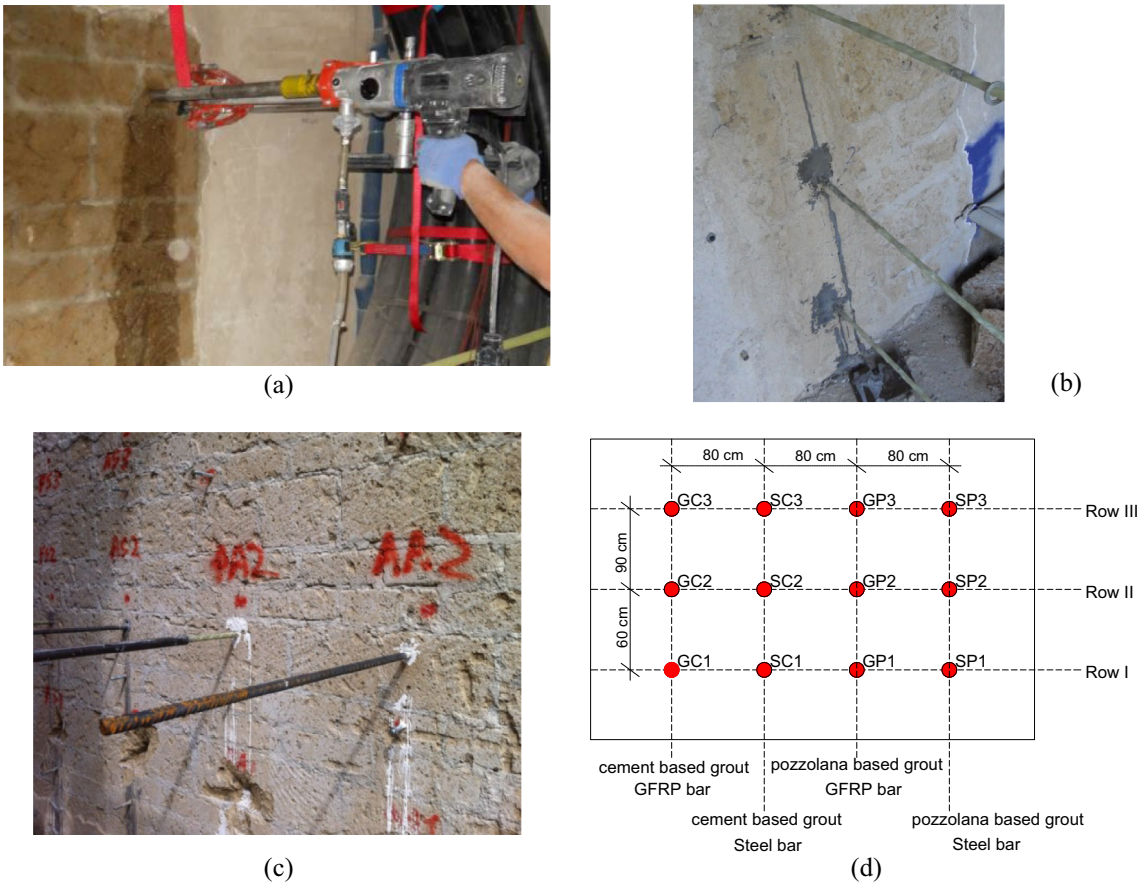

Fig. 2. a) Perforations for pull-out tests of series 1; b) 12 mm GFRP bars for pull-out tests of series 1; c) 20 mm steel and GFRP bars for pull-out tests of series 2; d) test matrix (values of spacing between bars refer specifically to tests of series 2).

be regarded as a type of consolidated pozzolana, and thus, the pozzolana-based grout is expected to have a very good physical-chemical compatibility with the tuff masonry.

The masonry walls were non-load-bearing elements inserted in a reinforced concrete frame consisting of only one floor; thus, they were subjected only to their own gravity load.

Two series of in situ pull-out tests were planned: the first series was planned as 'trial' set of tests for validating the experimental apparatus and concerned steel and glass bars with diameter $d_b = 12$ mm embedded in both types of grout. The second series concerned steel and glass bars with diameter $d_b = 20$ mm embedded in the same types of grout. In the first series the holes have diameter $d_g = 30$ mm and bonded length $l_e = 250$ mm (ratio $l_e/d_g = 8$), while in the second one the holes have diameter $d_g = 50$ mm and bonded length $l_e = 300$ mm ($l_e/d_g = 6$). The diameter of the borehole was chosen in both cases in order to have at least 10–15 mm around the bars and warrant the penetration of the grout in the borehole along the full length and the whole transversal section. Such a value corresponds also to attain the same borehole-to-bar diameter ratio, i.e. $d_g/d_b = 2.5$. In the second series the bonded length was increased (300 mm instead of 250 mm) to assure a higher safety factor respect to the current bonded length, since in some tests of the first series the bonded length resulted lower than the borehole length. Moreover, as the diameter increases the minimum bonded length requested for developing the full bond strength is expected to be higher. In both cases, the ratios l_e/d_g allow catalogue the anchors as 'medium-length' anchors (i.e. $5 < l_e/d_g < 15$, Algeri et al., 2010 [18]).

In both series, the boreholes were realized by realizing drillings (Fig. 2a) in the tuff blocks without intersecting the mortar joints in order to avoid any their influence. It is well known that in real applications the anchors should likely cross the mortar joints; in (Gigla, 2004 [16]) a corrective coefficient for evaluating the capacity of injected anchors is proposed for taking into account the presence of mortar joints by means of considering the effective contact area between the injected grout and the masonry blocks. However, in this experimental program such an issue has not been taken into account, but attention has been focussed on the other parameters previously discussed.

The position of the holes was planned to avoid interference between adjacent injections (Fig. 2b and c) and allow for the formation of a cone-shaped failure mechanism in the masonry caused by the pull-out force applied to each bar. In particular, the spacing between bars are in both series of tests larger than the provisions (2 times the bonded length) given by (MSJC, 2013 [26], ACI 318, 2011 [27]) for avoiding overlapping of the projected areas of adjacent anchors and, thus, for assuming no interaction: in particular, equal spacing of 800 mm in both directions for series 1, horizontal spacing of 800 mm and minimum vertical spacing of 600 mm for series 2; such values are equal or higher than 2 times the bonded length, i.e. 500 and 600 mm for series 1 and 2, respectively.

Particular care was taken during the injection phase in both series; in particular, water was first pumped into the boreholes before the grout was pressure-injected in order to wet the masonry surface and reduce the shrinkage of the grout. Despite of such care, in some cases the grout injection was imperfect and resulted in bonded length lower than the borehole length and/or in an incomplete filling of the space between the bar and the borehole. These defects were relieved after the bars were extracted from the masonry and have highlighted the strong

sensitivity of injected anchors performance to the *in-situ* application procedure.

For both types of series, the tests were labelled as follows: *B-G-n*, where *B* represents the Bar type (G for GFRP and S for Steel), *G* represents the Grout type (C for the Cement-based grout, named in the following as C-based grout, and P for the Pozzolana-based grout, named in the following as P-based grout) and *n* is the number of the row: e.g., S-P-1 indicates the test performed on the steel bar embedded in the P-based grout at row 1 (see the scheme reported in Fig. 2d valid for labels of tests of both series).

A specific counteract system was designed and implemented to prevent stress concentration in the masonry surrounding the bar and to allow for the eventual development of the cone-shaped failure surface in the masonry (Fig. 3a and b). The diameter of the contrasting tripod was about 620 mm. In the second series of tests, to avoid the slippage of the GFRP bars from the grips of the jack, which occurred in some tests of the first series, the anchoring system for loading the bars was improved. Being not possible to apply a high transversal pressure because of the low strength of the bars in the direction orthogonal to the fibres, a hollow steel cylinder with bolts was designed and constructed (Fig. 3c).

The pull-out force was applied by a cylindrical perforated jack placed coaxial to the bars and activated by a manual pump (maximum pressure 700 bar). A Linear Variable Displacement Transducer (LVDT) for measuring the slip between the bar and the masonry was placed at the loaded end of the bar for tests of the second series. The LVDT was placed between a fixed point on the jack and the unloaded end of the bar outside from the jack (Fig. 3a).

3.2. Mechanical properties of the materials

All materials used in the tests were experimentally tested to determine their mechanical properties. For each type of grout, compressive tests were performed on three cubes (50 mm on each side) corresponding to each row of injections.

For series 1, only one jet was realized for each type of grout and six cubes (side 50 mm) were realized as samples for mechanical characterization. The C-based grout was realized with a cement amount of 550 kg/m^3 and a water/cement ratio of 0.38, while for the P-based grout the water/pozzolana ratio was 0.35. The average experimental compressive strength, $f_{g,av}$, after 28 days of curing, was 82.9 MPa for the C-based grout and 22.9 for the P-based grout. Such values are listed in Table 1 (in italic) together with the Coefficient of Variation (CoV). Both the experimental values are slightly higher than the nominal values suggested by producer ($f_{g,nom}$ = 78.7 MPa and 18 MPa, for the C-based and the P-based grout, respectively).

For the second series, the C-based grout was realized with a lower content of cement (350 kg/m^3 with water/cement ratio 0.6) that led to have a lower nominal compressive strength (45.7 MPa). Three different jets were prepared, one for each row, and three cubes (side 50 mm) were realized for each jet. The values of $f_{g,av}$, after 28 days of curing, for each row are, thus, listed in Table 1 together with the corresponding CoV. The average strength computed considering the values of the three rows (in italic, 43.4 MPa) is comparable with the nominal one.

On the contrary, for the P-based grout of series 2, a larger amount of water was added in the mix, respect to the suggested one, in order to warrant fluidity and workability necessary for the injections and prevent the effect of evaporation because of the different environmental conditions respect to series 1 (the second series of tests was realized in summer). This led to have values of compressive strength sensibly lower than the nominal one (see Table 1) and to excluding the lowest value (i.e. 5.0 MPa, row II) from the calculation of the average strength (in italic, 12.6 MPa).

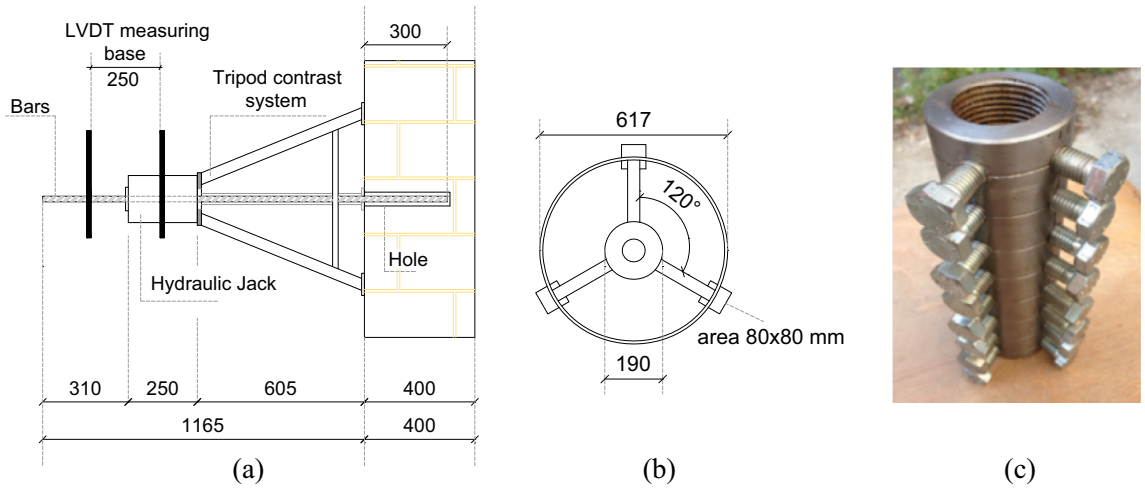

Fig. 3. Pull-out test equipment and instrumentation: a) tripod contrast system; b) detail of tripod base; c) detail of end gripping system used for bars of series 2 (measures in millimetres).

Table 1
Mechanical properties of grout for injections.

	Cement-based grout					Pozzolana-based grout				
	1st series	2nd series				1st series	2nd series			
		Row 1	Row 2	Row 3	Av.		Row 1	Row 2	Row 3	Av.
$f_{g,av}$ [MPa]	*82.9*	45.7	40.7	43.9	*43.4*	*22.9*	11.0	5.0*	14.3	*12.6*
CoV	6%	1.5%	27%	18%	16%	3%	7%	15%	11%	17%
$f_{g,nom}$ [MPa]	78.7	45.7				18.0				

* Not considered in the average value.

Compression tests were performed also on 8 cylinders made of undamaged tuff (samples of 50 mm in diameter and 50 mm in height) extracted from the boreholes of the second series of pull-out tests (Fig. 4). The experimental average compressive strength resulted 2.0 MPa with an acceptable scatter (CoV = 18%), nevertheless the intrinsic typical heterogeneity of tuff stone and despite the disturbance caused by the extraction from the holes.

Fig. 4. Tuff samples extracted from walls for compression tests.

Both types of steel bars (12 and 20 mm) used as anchors were conventional ribbed bars; the average experimental values of yielding, f_y, and ultimate stress, f_t, obtained by tensile tests on three samples for each type of bar are listed in Table 2 together with the corresponding CoV values.

Both types of GFRP bars were fabricated via a pultrusion process followed by the weaving of transverse glass fibres around the transversal section to produce spires with the intent of improving the bond along the surface (Fig. 5). The average values of tensile strength, f_t, and Young's modulus, E, given by experimental tensile tests carried out by the supplier are listed in Table 2.

In Tables 3 and 4 the variables analysed in such an experimental program (diameter of bar, d_b, diameter of borehole, d_g, bonded length, l_e, type of bar, type of grout, compressive strength of grout, $f_{g,av}$) are listed for tests of series 1 and series 2, respectively. Note that for the P-based grout of series 2, the average values of each row are listed due to the high variability of results, while for the C-based grout the average value of all rows is listed.

Table 2
Mechanical properties of steel and GFRP bars.

Anchor type	f_y [MPa]	f_t [MPa]	E [MPa]
Steel bar 12 mm	506	633	–
Steel bar 20 mm	448	551	–
GFRP bar 12 mm	–	990	48
GFRP bar 20 mm	–	1125	52

3.3. Experimental failure loads and modes for the pull-out tests of the series 1

In Table 3, the experimental pull-out forces applied to completely extract the bars from the masonry, F_{max}, are listed together with the corresponding failure modes and the efficiency factor η for each bar. The efficient factor is defined as $\eta = \frac{\sigma_{max}}{\sigma_t}$, being σ_{max}

Fig. 5. Detail of the 20 mm GFRP bars used in series 2.

Table 3
Results of pull-out tests of series 1.

Test	d_b [mm]	d_g [mm]	l_e [mm]	Grout	$f_{g,av}$ [MPa]	Bar	Failure	F_{max} [kN]	η	$F_{max,av}$ [kN]
SC_1	12	30	250	C	82.9	Steel	MCD + G/M	40.3	0.70	45.3 (16%)
SC_2							MCD + G/M	50.4	0.88	
SC_3							MCD + G/M	33.6*	0.59	
GC_1						GFRP	Failure of grips	47.0	0.42	44.5 (8%)
GC_2							Failure of grips	42.1	0.38	
GC_3							B/G	28.5*	0.26	
SP_1				P	22.9	Steel	B/G	47.0	0.82	47.3 (0%)
SP_2							B/G	47.5	0.83	
SP_3							MCD + steel bar yielding	58.8	1.03	58.8
GP_1						GFRP	B/G	33.6	0.30	37.3 (14%)
GP_2							Failure of grips	41.0	0.37	
GP_3							B/G	23.1*	0.21	

B/G: Bar-grout interface failure with complete slippage of the bar from the grout bulb.
G/M: Grout-masonry interface failure with pull-out of the bar and the surrounding grout bulb.
MCD: Masonry cone detachment.
C = Cement-based grout, P = Pozzolana-based grout.
* not considered in the average value because l_e was lower than 250 mm (100–150 mm).

the maximum stress in the bar at failure ($\sigma_{max} = \frac{F_{max}}{A}$), A the nominal transversal area of the bar, and σ_t the tensile strength of the bar (i.e. f_y for the steel bars and f_t for the GFRP bars). In addition, the average values of the pull-out forces, $F_{max,av}$, of the specimens of the same batch and failed in the same mode with the corresponding values of CoV are listed in Table 3.

3.3.1. Behaviour of steel bars

In the tests with steel bars embedded in the C-based grout, a cone shape masonry failure (MCD) occurred coupled with the grout/masonry interface failure (Fig. 6a); the efficiency factors range in 70–90%, with exception of the bar SC_3 that attained a lower failure load (33.6 kN) due to the reduced bonded length (l_e = 150 mm), as it was evidenced after the complete extraction of the bar (Fig. 6d).

When the steel bars were embedded in the P-based grout, in two cases the complete slippage of the bar from the grout bulb occurred (B/G, Fig. 6b) with maximum loads practically coincident and slightly higher than the ones attained in the case of C-based grout (+5%, $\eta \approx 80\%$). Conversely, for the third bar, SP_3, both cone shaped masonry failure and yielding of the bar occurred at an even higher load (58.8 kN, $\eta \approx 100\%$, +30% compared with the case of the C-based grout). These results show that:

1) the bond strength of the steel bar/P-based grout interface is weaker than the one of the steel-bar/C-based grout, due both to the lower mechanical properties of the P-based grout and to its worse chemical-physical compatibility with the steel bar surface; the bar-grout interface failure occurred, indeed, for two steel bars embedded in the P-based grout, while the masonry failure occurred for all the steel bars embedded in the C-based grout at comparable loads (47.3 vs. 45.3 kN);
2) the P-based grout transfers lower tensile stresses to the masonry around the injected anchor respect to the C-based one, probably due to its lower stiffness; the masonry failure occurred, indeed, in only one case, but at higher loads (+30%), while the bar-grout interface failure occurred before masonry failure for the other two bars;
3) the cone shaped masonry failure was attained at sensibly different loads for the steel bars embedded in the P-based and the C-based grout; this means that it depends both on the bond stresses transferred by the injected anchor and on the local physical and mechanical properties of the masonry around it.

3.3.2. Behaviour of GFRP bars

For the GFRP bars embedded in the C-based grout, failure of anchoring grips occurred in two cases shortly before failure of masonry; the maximum loads attained in these two tests (42–47 kN) were in the same range of values (40–50 kN) attained in the tests on the steel bars embedded in the same grout. On the contrary, for specimen GC_3 the complete slipping of the GFRP bar from the grout occurred due to the shorter bonded length relieved after the test (about 150 mm) and, thus, the lower load attained (28.5 kN) was not considered in the average. It is worth to note that, nevertheless the similar failure loads attained in the tests, the efficiency factors of the GFRP bars were lower than the steel bars ($\eta \approx 40\%$), due to the higher tensile strength of the first ones. However, because the failure of the anchoring grips occurred before the masonry cone shaped failure and the bar-grout interface failure, the experimental maximum loads may represent an underestimation of the effective failure loads.

For two GFRP bars embedded in the P-based grout the bar/grout interface failure occurred and the grout bulb remained completely

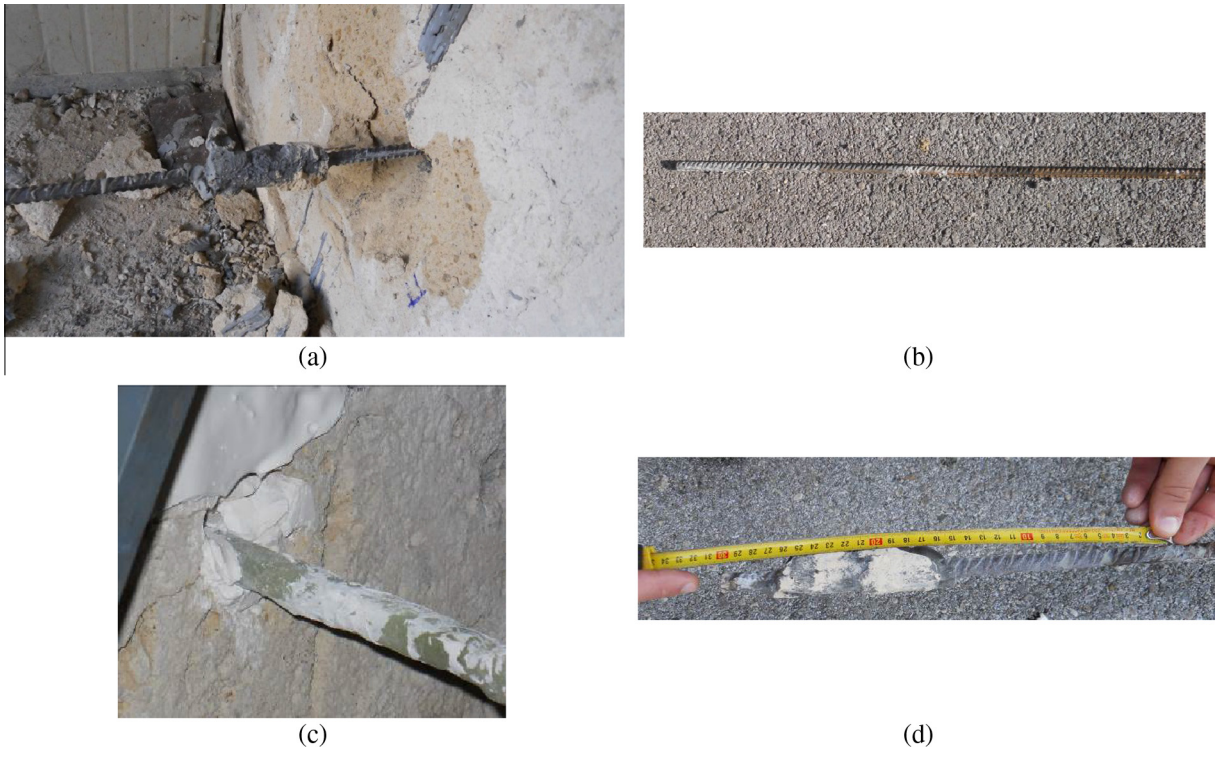

Fig. 6. Typical failure modes observed in series 1: a) Masonry Cone Detachment (MCD) for steel bar embedded in C-based grout; b) complete slippage of the steel bar embedded in the P-based grout after the test (B/G failure); c) Bar/Grout (B/G) interface failure for the GFRP bar embedded in the P-based grout; d) bonded length of 150 mm for bar SC_3 relieved after the pull-out test.

inside the masonry (Fig. 6c); for one of these two bars (GP_3) the reduced bonded length observed after the test induced a significant lower failure load (23.1 kN). Conversely, only for the bar GP_2 the bond strength at the bar-grout interface was higher and the failure of grips occurred at a load sligthly lower than the ones attained in the case of C-based grout for the same grips failure.

These results highlight two critical issues for the GFRP bars:

1) the low reliability of the anchoring grips that needs to be improved;
2) the worse bond behaviour activated along the bar-grout surface, especially in case of the P-based grout; this was due both to the lower strength of the P-based grout, which has induced a bar-grout interface failure in several cases, and to a less effective interlocking of the GFRP bar surface. The different bond behaviour and failure mechanisms activated in GFRP bars embedded in concrete elements are well known (Pecce et al., 2001 [41]).

The first trial series of pull-out tests has also confirmed a typical critical issue of the injected anchors: the uncertainness about the effective value of the bonded length that depends on chemical, physical and rheological properties of the grout, on the pressure used for injecting the grout, and on the cracking and damage status of the masonry around the hole. This may lead to consider higher safety factor to take into account the uncertain quality of realization. For these reasons the second series of pull-out tests was realized adopting a longer bonded length (300 mm instead of 250 mm) and a more fluid grout for facilitating the injection and the complete filing of the space between bars and masonry.

3.4. Experimental failure loads and modes for the pull-out tests of the second series

In Table 4, the same data of Table 3 are listed with refer to the pull-out tests of series 2. In the following sections the results of series 2 are discussed in detail with refer to the different behaviour of steel and GFRP bars embedded in the two types of grout, i.e. the cement-based and the pozzolana-based ones, used in the second part of the experimental program.

3.4.1. Behaviour of bars embedded in the pozzolana-based grout

Both steel and GFRP bars embedded in the P-based grout exhibited complete extraction of the bar from the grout (failure at the bar-grout interface, B/G), while the grout bulb remained inside the borehole (see Fig. 7a and b), evidencing the same criticism already evidenced in the first series of tests. It is worth to note that the bar GP_2 was characterized by a not complete filling of the hole because of the excessive fluidity of the grout mix used for row II that, indeed, determined also the very low strength of the grout for such a row; thus, the maximum load of bar GP_2 has not been considered for calculating the average value. Although steel and GFRP bars exhibited the same failure mode, the average maximum load achieved by the GFRP bars was lower (33 kN) than that achieved by the steel bars (45–50 kN, i.e. −30%). This can most likely be attributed to the less efficient surface roughness of the GFRP bars compared with the ribs of the steel bars, as already highlighted by tests of series 1. Moreover, the very low strenght of the grout mix of row 2 did not influence significantly the maximum pull-out force of the steel bar (SP_2), evidencing, thus, that the higher interlocking capacity of the steel bars compensates for the reduced strenght of the grout. For both types of bars, the CoV values were negligible (2–5%) and the extent of exploitation of the material properties was quite low (η = 32–36% and 9% for steel and GFRP bars, respectively). Again, the very low values of η for the GFRP bars are related both to their worse performance and higher tensile strength compared with the steel bars.

3.4.2. Behaviour of bars embedded in the cement-based grout

For the steel bars embedded with the C-based grout, the complete pull-out of the bar and the surrounding grout bulb (G/M, Fig. 7c) occurred coupled with the detachment of a cone-shaped volume of masonry (MCD) contained inside the external diameter of the contrasting tripod. The maximum loads ranged from 50 to 65 kN, indicating an average increase in the pull-out force of approximately 20% compared with the case of the same bars embedded in the P-based grout; also the efficiency factors were, thus, higher (η = 35–46%). This load increase can most likely be attributed to the superior mechanical properties and the lower fluidity of the C-based grout compared with the P-based mix realized in series 2. However, the more complex failure mechanism, which involved both the bar-grout and the grout-masonry interface, led to a higher scatter in the results of the steel bars when the C-based grout is used instead of the P-based one (i.e. CoV = 13% vs. 5%).

Moreover, for the GFRP bars embedded in the C-based grout, an even more significant increase in the pull-out force was observed in comparison with the use of the P-based grout (up to +60%); this led also that the average maximum load was only 8% lower than the value attained by the steel bars embedded in the C-based grout. Despite such a significant load increase, the failure did not involve the complete detachment of the grout bulb, as observed for the

Table 4
Results of pull-out tests of series 2.

Test	d_b [mm]	d_g [mm]	l_e [mm]	Grout	$f_{g,av}$ [MPa]	Bar	Failure	F_{max} [kN]	η	$F_{max,av}$ [kN]
SC_1	20	50	300	C	43.4	Steel	G/M + MCD	57.0	0.40	57.2 (13%)
SC_2							G/M + MCD	65.0	0.46	
SC_3							G/M + MCD	49.7	0.35	
GC_1						GFRP	B/G + G/M + MCD	46.6	0.13	52.6 (11%)
GC_2							B/G + MCD	53.8	0.15	
GC_3							B/G + MCD	57.4	0.16	
SP_1				P	11.0	Steel	B/G	50.4	0.36	47.6 (5%)
SP_2					5.0		B/G	47.0	0.33	
SP_3					14.3		B/G	45.6	0.32	
GP_1					11.0	GFRP	B/G	33.3	0.09	32.9 (2%)
GP_2					5.0		B/G	24.0*	0.07	
GP_3					14.3		B/G	32.5	0.09	

B/G: Bar-grout interface failure with complete slippage of the bar from the grout bulb.
G/M: Grout-masonry interface failure with pull-out of the bar and the surrounding grout bulb.
MCD: Masonry cone detachment.
C = Cement-based grout, P = Pozzolana-based grout.
* Not considered in the average value due to a not complete filling of the borehole.

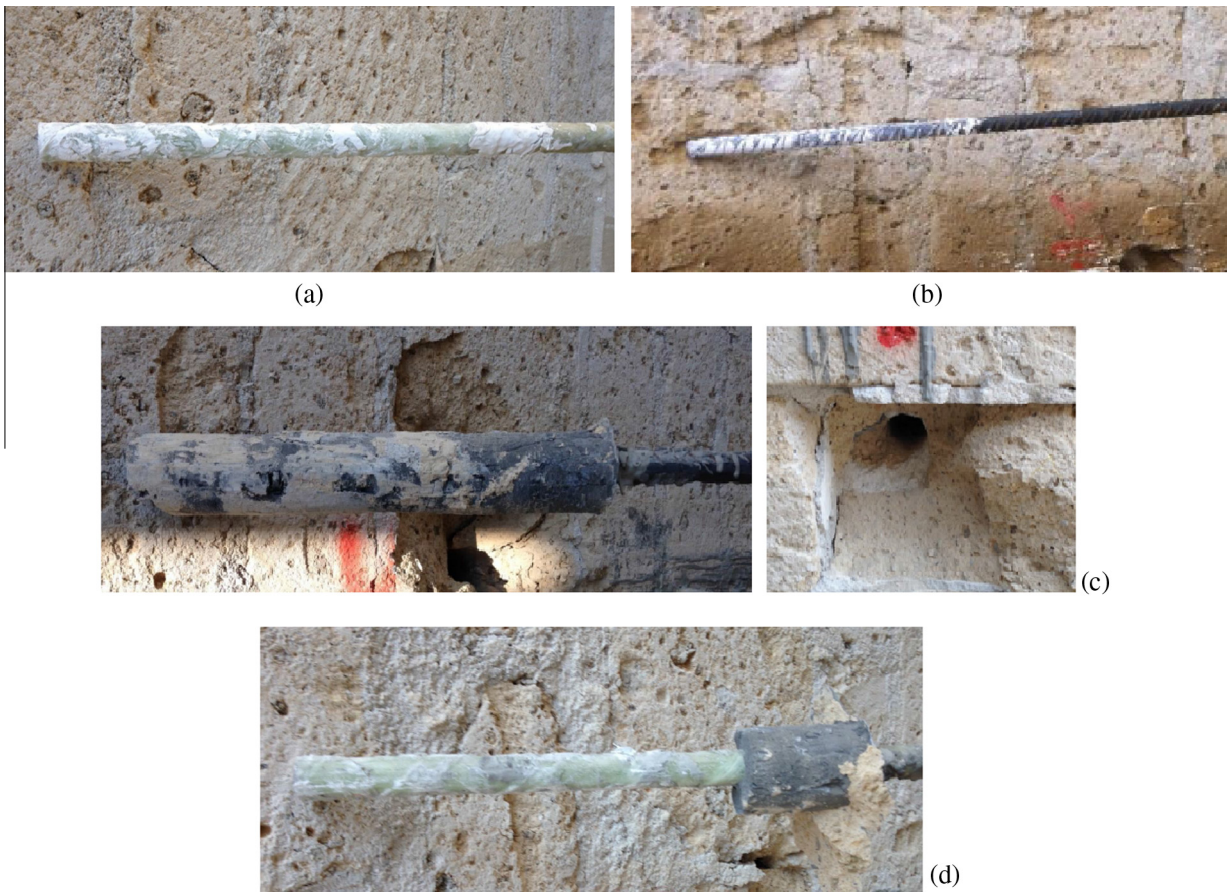

Fig. 7. Typical failure modes observed in series 2: a) Bar/Grout (B/G) interface failure for GFRP bar in P-based grout; b) Bar/Grout (B/G) interface failure for steel bar in P-based grout; c) Grout/Masonry (G/M) interface failure with the Masonry Cone Detachment (MCD) for steel bar in C-based grout; d) mixed Bar/Grout and Grout/Masonry interface failures with partial Masonry Cone Detachment (B/G + G/M + MCD) for GFRP bar in C-based grout.

steel bars; instead, a mixed failure mode occurred, with the slipping of the bar along the bar-grout interface and a partial detachment of the grout bulb (Fig. 7d). Again, the more complex failure mode induced a higher scatter of the results when the C-based grout is used (CoV = 11% vs. 2%).

3.5. Comparison of results of the two series

3.5.1. Effect of grout

The results of pull-out tests of series 2 have highlighted that the C-based grout allows attained the best performance both for steel and GFRP bars with slight differences for the two types of bars (8%). In the tests of series 1, comparable maximum loads were attained for the steel and GFRP bars embedded in the C-based grout. Moreover, the failure loads attained in series 2 were higher than the value of series 1 (i.e. +26% for the steel bars and +18% for the GFRP bars), but the efficiency ratios are about the half, due to the combined effect of the higher bar diameter, the lower strength of the C-based mix, and the masonry strength that was the same in the two series. The compressive strength of the C-based grout of series 2 was, indeed, almost the half of the value used in series 1 in order to reduce the stiffness of the grout and trying to delay to higher loads the masonry failure occurred in series 1. Moreover, a too high strength for the grout is not necessary also because the strength of the masonry surrounding the anchor influences the upper limit of the maximum pull-out force.

Both series of tests have evidenced that the use of the P-based grout is particularly detrimental for the GFRP bars since they attained sensibly lower failure loads compared with the steel bars ($-20 \div 35\%$ in series 1 and -30% in series 2). On the contrary, the steel bar embedded in the P-based grout attained loads comparable with those of the C-based one in the tests of series 1, while a load reduction of only 20% was achieved in series 2. It is worth also to note that the lower strength (12.7 MPa vs. 22.9 MPa) and the higher fluidity of the P-based grout used in series 2 has probably negatively influenced the performance of both steel and GFRP bars. Differently from the trend observed for the C-based grout, the maximum loads attained in series 2 were, indeed, lower than the values of series 1, nevertheless the higher diameter and the same masonry strength (-20% for the steel bars, -12% for GFRP bars). Moreover, for both types of bars embedded in the P-based grout, the predominant failure mode observed in both series was the bar-grout interface one, which is, in general, significant of the lower bond strength of the P-based grout compared to that of the C-based one. The lower compressive strength of the P-based grout is also significant of a lower stiffness that may have a positive effect into reducing concentration of bond shear stresses in the masonry surrounding the anchor. In the tests on the steel bars of series 1 the failure loads were, indeed, practically coincident for the two types of grout and, in the case of the P-based grout, the cone shape masonry was even activated. The same did not occur for the steel bars in the tests of series 2, not only because of the worse quality of the P-based mix realized in such series, as previously discussed, but also because of the influence of different values of bar diameter d_b, borehole diameter, d_g, i.e. grout bulb diameter, and l_e/d_g ratio, as discussed in the following.

Moreover, the coupling GFRP bars/P-based grout attained the worst performances in both series; this was mainly due to a lower

interlocking effect produced by the surface treatment of the GFRP bars (twisted glass fibres glued along the bar surface) compared with the traditional ribs of the steel bars and a lower chemical compatibility. This probably avoided to attain comparable results for the two types of bar in series 1 and led to have a further detrimental effect on the global performance when the lower strength P-based grout was used in series 2. Some comments about the different bond behaviour of the two types of bars embedded in the two grout mixtures are reported in Section 3.6.

As further comment about the influence of the mechanical properties of the grout, it worth to note that several studies are available in literature (Valluzzi et al. 2004 [10]; Silva et al., 2014 [42]; Vintzileou and Miltiadou-Fezans, 2008 [13]) about the effect of grout injections into enhancing the behaviour of multi-leaf stone masonry elements (i.e. mainly aimed to fill voids and cracks, consolidate poor strength filling materials between leaves, improve the mechanical properties of the overall masonry assembly, and enhance the connections between the leaves). In particular, it was highlighted (Silva et al., 2014 [42]) that when the grout-to-masonry strength ratio becomes higher than 5, the influence on the increased load capacity of the masonry walls is very little; conversely, lower strength lime-based grouts are more compatible both on the mechanical and physical point of view and a better exploitation of their mechanical properties is attained. However, for the injected anchors, the global performances of the intervention are influenced not only by the interaction of the grout with the surrounding masonry, but also by the interaction with the anchor system, i.e. its surface treatment and chemical compatibility.

3.5.2. Effect of bar diameter

As previously observed, for the C-based grout the failure loads achieved in series 2 (characterized by $d_b = 20$ mm, $d_g = 50$ mm, $l_e/d_g = 6$) were greater than the ones of series 1 ($d_b = 12$ mm, $d_g = 30$ mm, $l_e/d_g = 8$); such a load increase (+26% and 18% for the steel and GFRP bars, respectively) is, however, not proportional to the diameter variation and led to lower exploiting rates of the bar tensile strength: $\eta = 0.38–0.88$ in series 1 and $\eta = 0.13–0.46$ in series 2. If the bond shear strength was the same in the two series, the maximum pull-out force should be directly proportional to the bonded surface, i.e. to the bar diameter. In reality, the bond strength is not the same since the compressive strength of the C-based grout of series 2 is lower than the one used in series 1. Moreover, the anchor performances strongly depend also on the masonry strength, which was the same for the two series of tests and represents the same upper limit for the anchor strength capacity for whatever bar diameter and grout strength. Finally, since greater diameters mean higher bonded surface, the transfer of the bond shear stresses to the surrounding grout and masonry exhausts in a shorter distance; such a more concentrated shear stress distribution, in case of materials with low tensile strength, may also lead to lower failure load increase. All these factors contributed to the not proportional increase of the failure load with the diameter variation.

Conversely, for the P-based grout, the maximum loads attained in series 2 were lower than the values attained in series 1 (−20% for the steel bars, −12% for GFRP bars and, thus, the efficiency factors were even lower than the values attained in series 1); in addition to the already discussed effect of the lower strength of the P-based grout of series 2, such results may be ascribable also to the effect of the larger bar and borehole diameter and to the lower l_e/d_g ratio. The first series was characterized by a higher ratio l_e/d_g (8 vs. 6) and the anchor strength is expected to increase as longer as the bonded length is for the same bar or borehole diameter and, in general, for larger values of l_e/d_g. Moreover, because the transfer length of the bond shear stresses usually increases as the bar diameter and the bond shear strength decrease, the bonded length in the pull-out tests should be increased as the bar diameter and the bond shear strength, i.e. the tensile strength of bonded materials (grout and masonry), decrease. For the bars of series 2 embedded in the P-based grout, the effect of higher diameter is contrasted by the effect of the lower grout strength; thus, the value of $l_e/d_g = 6$ is probably too short and, indeed, a bar/grout interface failure occurred.

3.6. Bond shear stress-slip relationships

The various contributions to the bond behaviour are represented by different regions of the shear stress-slip relation: initially, as the stresses increase, no slip is expected between the bar and grout because of the physical-chemical adhesion. As the load increases, a stress concentration develops in the grout around the bar and leads to the beginning of slips without cracking. During this phase, which is governed by friction, strength and stiffness can be improved by interlocking phenomena and by presence of stresses transversal to the bar. The occurrence of slip also depends on the interaction along the grout-masonry substrate interface and, thus, on the ramification of the injected grout in the masonry microstructure. When cracks begin to form in the grout, the bond relation becomes less stiff and is governed by friction and by interlocking of the inclined struts formed in the grout. To highlight such phases, in Figs. 8–10 the experimental shear stress-displacement curves are reported for the pull-out tests of series 2. The shear stress, τ_b, is the average value along the bonded surface of the bar, S_b, calculated as follows:

$$\tau_b = \frac{F}{S_b} \quad S_b = \pi \cdot d_b \cdot l_e \tag{1}$$

being F the tensile force applied to the bar during the test, d_b the diameter of the bar (20 mm) and l_e the embedded bonded length (300 mm). The displacement is given by the LVDT measures.

In Fig. 8, the experimental τ_b-s curves for the steel and GFRP bars injected with the P-based grout are plotted. The two available curves for the GFRP bars indicate deformability greater than those for the steel bars, with exception of the steel bar SP_2 that was characterized from the beginning of the test by very high slips. For the steel bars, the slips were negligible for stresses in the range of 1.1–1.6 MPa (20–30 kN) and then began to significantly increase, whereas for the GFRP bars, the range of zero slip was lower, i.e., 0.5–1.1 MPa (10–20 kN). The initial condition of negligible slip is attributable to the chemical adhesion between the grout and the bars; when this adhesion is overcome, the aggregate interlocking mechanism is activated. Thus, the lower performance of the GFRP bars in terms of stiffness and strength can be ascribed both to the lower chemical compatibility of these bars with the grout and to the less effective interlocking effect produced by the twisted glass fibres along the surfaces of these bars.

Analogously, in Fig. 9, the experimental τ_b-s curves for the steel and GFRP bars injected with the C-based grout are plotted. Unlike the behaviour observed in Fig. 8, no initial range with zero slip is clearly identifiable for either type of bars, suggesting that the physical-chemical adhesion of the C-based grout is worse than that observed for the P-based grout. On the contrary, the higher pull-out forces achieved in the case of the C-based grout seems mainly due to the interlocking mechanisms activated after the physical-chemical adhesion threshold is overcame. Fig. 9 also shows that the GFRP bars again exhibited greater deformability throughout the entire load history, indicating that the lower roughness of their surfaces has a detrimental effect on both the initial adhesion and the subsequent phases.

In Fig. 10a and b, the experimental τ_b-s curves are plotted for the steel bars embedded in the two types of grout (Fig. 10a) and analogously for the GFRP bars (Fig. 10b). In general, the P-based

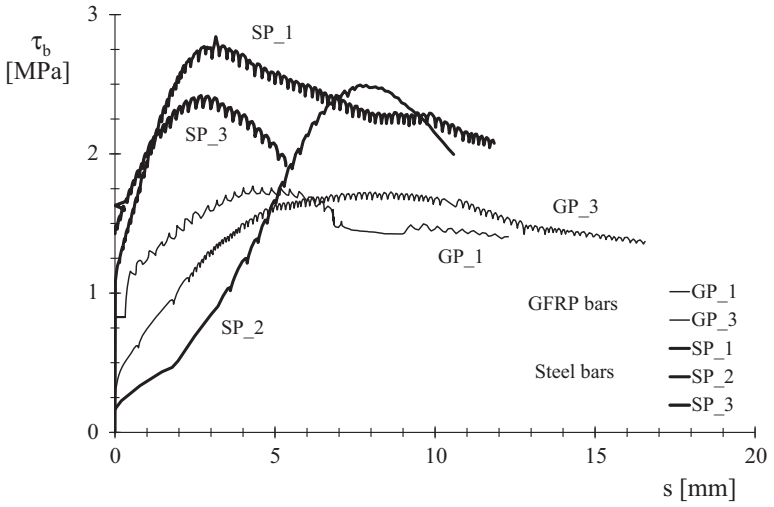

Fig. 8. Experimental shear stress-slip relations for steel and GFRP bars of series 2 injected with P-based grout.

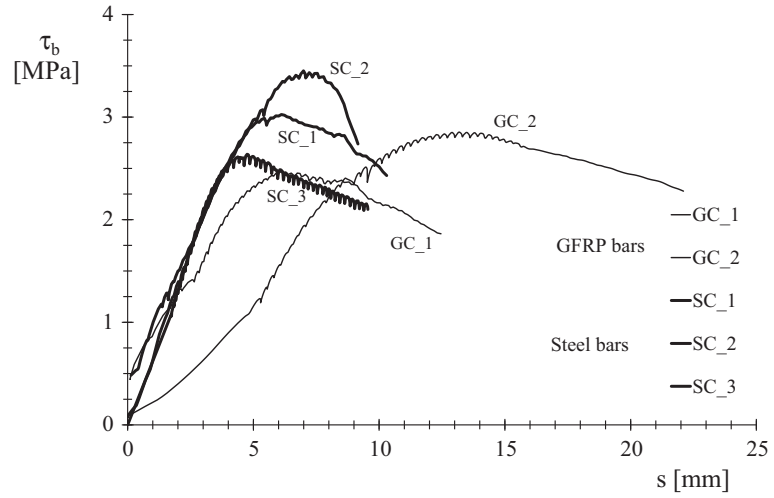

Fig. 9. Experimental shear stress-slip relations for steel and GFRP bars of series 2 injected with C-based grout.

grout allowed for lower slip compared with the C-based grout for both the steel (Fig. 10a) and GFRP bars (Fig. 10b) at the beginning of the loading history. The P-based grout offers, thus, a better chemical adhesion at low load levels, while, after the adhesion strength is overcome, the less effective mechanical interlocking leads to attain comparable slips and lower pull-out strengths. By contrast, the C-based grout appears to provide superior mechanical interlocking, as evidenced by the higher pull-out load and the larger volume of material involved in the failure mechanism (total or partial detachment of the grout bulb and the detachment of a cone-shaped volume of masonry). In Table 5 the values of the maximum average shear stresses, calculated as $\tau_{b,\max} = \frac{F_{\max}}{S_b}$, and the parameter β, defined as the ratio of $\tau_{b,max}$ to the average experimental compressive strength of the grout, $f_{g,av}$ (see the average experimental values listed in Table 1) are reported for the results of both series of pull-out tests. Note that for some bars, indicated with asterisk in Table 5, $\tau_{b,max}$ is calculated with refer to a lower values of l_e, i.e. 150 mm, as it was evidenced after the complete extraction of bar from masonry (Fig. 6d).

The parameter β is significant to show the level of exploiting of the grout strength as the failure mode changes. Table 5 highlights that for the bars of series 2 embedded in the P-based grout, which always failed at the bar-grout interface, the parameter β is about 0.14 for the GFRP bars and 0.20 for the steel bars; slightly higher values of β have been obtained for the bars of series 1: 0.22–0.27 for the steel bars that has a mixed MCD and B/G interface failure and 0.15–0.19 for the GFRP bars that had a B/G interface failure. Considering that for the P-based grout the bar/grout interface failure occurred in most cases, such values of β may indicate that the shear bond strength of the bar/P-based grout interface is in average 20% of the grout compressive strength, even if higher exploitation ratios of the grout strength have been attained for the steel bars compared with the GFRP bars. Such a correlation is, indeed, too simple, since the bar surface configuration (i.e., for the case at hand, traditional ribs for steel bars and twisted glass fibres for the GFRP bars) and the grout composition should be taken into account. The surface treatment of the bar certainly influences the shear strength and, in particular, affects the contribution due to mechanical interlocking induced by ribs or twisted fibers along the bar surface, whereas the ramification of the grout within the masonry and, thus, the damage status of the masonry (cracks, voids, etc.) influences the interlocking along the grout-masonry interface. About the effect of grout composition, it may be as more significant as lower the grout strength is; for the same type of bars,

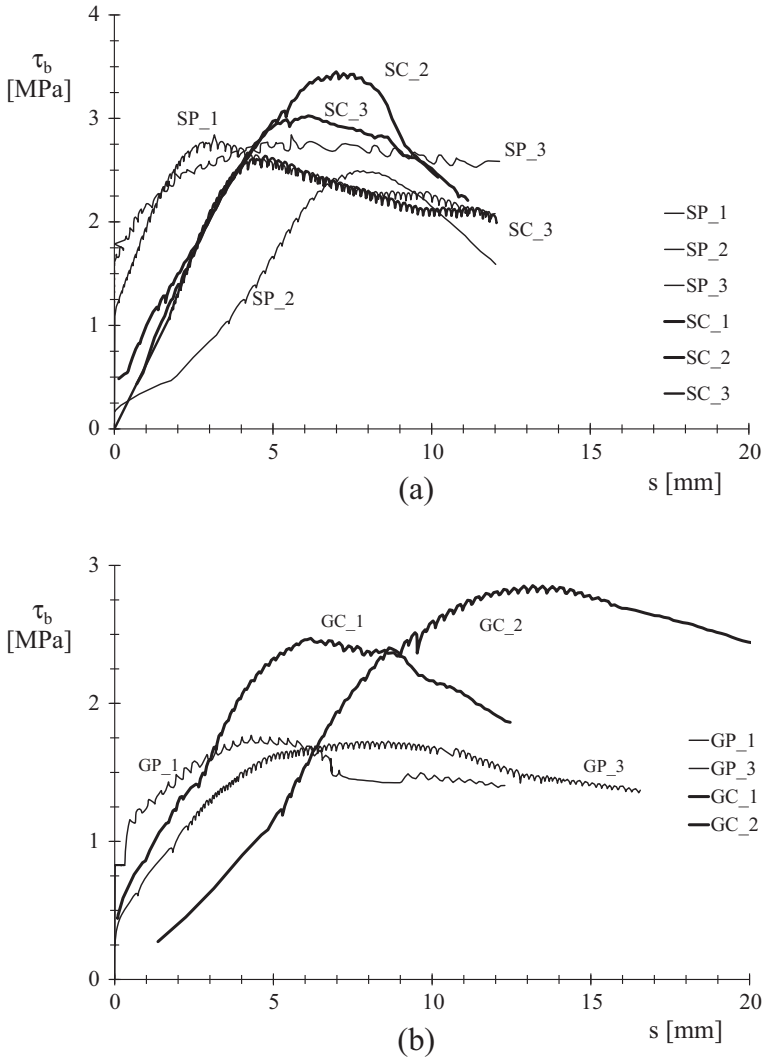

Fig. 10. Comparisons of experimental shear stress-slip relations for bars of series 2 embedded in P-based and C-based grout: a) steel bars; b) GFRP bars.

Table 5
Experimental values of shear stresses for pull-out tests.

Series 1						Series 2					
Test	Grout	Bar	F_{max} [kN]	$\tau_{b,max}$ [MPa]	β	Test	Grout	Bar	F_{max} [kN]	$\tau_{b,max}$ [MPa]	β
SC_1	C	Steel	40.3	4.3	0.05	SC_1	C	Steel	57.0	3.0	0.07
SC_2			50.4	5.4	0.06	SC_2			65.0	3.5	0.08
SC_3			33.6*	5.9	0.04	SC_3			49.7	2.6	0.06
GC_1		GFRP	47.0	5.0	0.06	GC_1		GFRP	46.6	2.5	0.06
GC_2			42.1	4.5	0.05	GC_2			53.8	2.9	0.07
GC_3			28.5*	5.0	0.04	GC_3			57.4	3.1	0.07
SP_1	P	Steel	47.0	5.0	0.22	SP_1	P	Steel	50.4	2.7	0.21
SP_2			47.5	5.0	0.22	SP_2			47.0	2.5	0.20
SP_3			58.8	6.2	0.27	SP_3			45.6	2.4	0.19
GP_1		GFRP	33.6	3.6	0.15	GP_1		GFRP	33.3	1.8	0.14
GP_2			41.0	4.4	0.19	GP_2			24.0**	1.3	0.10
GP_3			23.1*	4.1	0.11	GP_3			32.5	1.7	0.14

C = Cement-based grout, P = Pozzolana-based grout.
* Bars with reduced embedded length (l_e = 150 mm).
** Borehole section non completely filled by grout.

β is, indeed, lower for the poorer P-based mix of series 2, meaning that β decreases as lower is the grout compressive strength.

When the C-based grout is used, a lower exploiting of the grout strength is achieved, obviously because of the very high compressive strength of such a grout (82.9 and 43.4 MPa); β is, indeed, about 0.05 for both types of bars of series 1 and about 0.07 for both types of bars of series 2. The lower exploiting of the C-based grout reflected also in the failure mode that moved from the bar/grout interface to the grout/masonry interface and involved often also the masonry surrounding the bars in both series of tests.

Differently from the P-based grout, the comparable values of β attained for the C-based grout in the two series show that the use of a lower strength grout did not have an influence on the rate of exploiting of the grout strength, probably because the compressive strength of the C-based grout of series 2 is however very high (i.e. 43 MPa that is about 3.6 times the strength of the P-based grout used in the same series, 12.6 MPa).

4. Comparison of experimental pull-out forces with literature formulas

4.1. Cone masonry detachment

The formulas for predicting the failure mode known as "masonry break-out" or "cone-shaped masonry" failure are all based on the compressive strength of the masonry, f_m, and on the embedded length of the anchor, l_e. Some formulations are listed in the following:

a) ACI 318 [27]; *fib* 58 [36]

$$N = 4.1 \cdot l_e^{1.5} \cdot \sqrt{f_m} \tag{2}$$

b) MSJC [26]

$$N = 0.332 \cdot \pi \cdot l_e^2 \cdot \sqrt{f_m} \tag{3}$$

c) CEB [39]

$$N = 0.85 \cdot l_e^2 \cdot \sqrt{f_m} \tag{4}$$

d) Arifpovic and Nielsen [34]

$$N = 0.96 \cdot (d_b + l_e) \cdot l_e \cdot \sqrt{f_m} \tag{5}$$

It is worth to note that some of these formulas (i.e., ACI 318 [27] and *fib* bulletin 58 [36]) were originally assessed for steel bars embedded in concrete elements and, then, have been assessed also for predicting strength of anchors in masonry elements. In Table 6, the predicted values given by these formulations for the pull-out tests of series 1 and 2 using f_m = 2 MPa and l_e = 250 and 300 mm are reported.

Note that in the formulation of ACI 318 [27], i.e. Eq. (2), there are several factors, which are not reported herein for the sake of simplicity, that depend on the overlapping areas of adjacent anchors, splitting, and edge effects; because none of these effects were observed in the present experiment, all these factors can be assumed to be equal to 1. Such an assumption leads also to have that the *fib* prediction [36] is the same as that of ACI 318 [27] and both of them can be expressed by Eq. (2). The predictions given by Eq. (2) underestimate significantly the average experimental failure loads of both series; i.e. of about 40–60% for series 1 and 10–50% for series 2. It is worth to note that the worst underestimations are attained just for the tests where the cone shape masonry failure occurred alone or coupled with other failure modes since the experimental failure loads associated to such failure modes were sensibly higher than the predicted values (see for example the failure load of specimen SP_3 of series 1, 58.5 kN, and of the steel bars with C-based grout of series 2, 57.2 kN).

Table 6
Comparison between experimental and theoretical pull-out forces for cone-shaped masonry failure.

Series	Grout	Series	Bar	$F_{max,av}$ [kN]	Theoretical values, Fth [kN]			
					Eq. (2)	Eq. (3)	Eq. (4)	Eq. (5)
1	C	SC	Steel	45.3				
		GC	GFRP	44.5				
	P	SP_1/SP_2	Steel	47.3	22.9	92.1	75.1	106.7
		SP_3	Steel	58.8*				
		GP	GFRP	37.3				
2	C	SC	Steel	57.2				
		GC	GFRP	52.6	30.1	132.7	108.2	130.3
	P	SP	Steel	47.6				
		GP	GFRP	32.9				

* specimen failed for Masonry cone Detachment + steel bar yielding.

On the contrary, all other theoretical formulations significantly overestimate the experimental results, as also found in (Araujo et al., 2014b [43]). In particular, predictions of Eq. (3) (MSJC, 2013 [26]) are from 1.6 to 2.4 times higher than the average experimental values for series 1 and from 2.3 to 4.0 times higher for series 2; predictions of Eq. (4) (CEB, 1994 [39]) are from 1.3 to 2.0 times higher for series 1 and from 1.9 to 3.3 higher for series 2; predictions of Eq. (5) (Arifpovic and Nielsen, 2006 [34]) are from 1.8 to 2.9 times higher for series 1 and from 2.3 to 4.0 times higher for series 2.

Note that in (MSJC, 2013 [26]), a minimum bonded length, l_e, for the injected anchors is suggested as the maximum value between 51 mm and 4 times the diameter of the anchor. For the pull-out tests of series 1 (d_b = 12 mm), thus, the minimum suggested value of the bonded length is 51 mm, while for the tests of series 2 (d_b = 20 mm) is 80 mm; in both cases these values are shorter than the actual embedded length used in the tests (250 and 300 mm, respectively). However, these minimum values may be not safe for warranting the maximum bond strength of the anchor is achieved, because it was experimentally observed that, when the actual embedded length resulted lower than the planned one (about 150 mm instead of 250 or 300 mm, see cases indicated with asterisk in Tables 3 and 4), the maximum pull-out force sensibly decreased.

4.2. Bond failure modes

Most literature strength models give predictions for a mixed failure mode in which cone-shaped masonry failure is accompanied by slippage along the outer (grout-masonry) interface; such a failure mode is also generically known as 'bond' failure. Other formulas provide specific indications for bond failure at the bar-grout or grout-masonry interface, depending on the bonded surface under consideration. The following formulations for the bond and mixed failure modes have been considered for comparison with the experimental results:

a) Gigla and Wenzel [30] – Bond failure (failure at bar/grout interface)

$$N = \tau_u \cdot S_b \quad S_b = \pi \cdot d_b \cdot l_e \tag{6}$$

b) Arifpovic and Nielsen [34] – Bond failure (failure at bar/grout interface)

$$N = 3.79 \cdot d_b \cdot l_e \cdot \sqrt{f_m} \tag{7}$$

c) CEB [39] – ACI 318 [27] – fib 58 [36]
Bond failure (failure at grout/masonry interface)

$$N = \tau_u \cdot S_g \quad S_g = \pi \cdot d_g \cdot l_e \tag{8}$$

d) Cook et al. [35] – Mixed failure (Masonry cone detachment + bond failure)

$$N = \frac{34.7 \cdot \pi \cdot \tau_u \cdot d_b^{1.5}}{\lambda} \cdot \tanh\left[\frac{\lambda \cdot (l_e - 50)}{34.76 \cdot d_b^{0.5}}\right] \quad \lambda = 0.3 \tag{9}$$

e) Arifpovic and Nielsen [34] – Mixed failure (Masonry cone detachment + bond failure)

$$N = \left[3.93 \cdot \sqrt{f_m} \cdot (l_e - 5.76 \cdot d_b) \cdot d_b + 37.44 \cdot \sqrt{f_j} \cdot (l_u + d_b) \cdot d_b\right] \cdot \sqrt{\frac{d_b}{l_e}} \quad (10)$$

Most of these formulations introduce in the prediction of the maximum pull-out force the bond shear strength, τ_u, and refer to the following formulation suggested by (Gigla and Wenzel, 2000 [30]):

$$\tau_u = \Phi_j \cdot \frac{f_g^2}{500}, \Phi_j = 0.6 \quad (11)$$

being f_g the compressive strength of the grout.

Also for the formulations predicting bond failures, because there is no interactions between adjacent anchors, splitting or edge effects, the formulas of ACI 318 [27] and *fib* bulletin 58 [36] can be simplified and they become analogous to the simple expression given by CEB [39] (Eq. (8)). Note that none of these expressions directly accounts for the surface properties of the anchor systems.

The values of τ_u predicted by Eq. (11) are equal to 0.63 MPa and 8.25 MPa for the P- and C-based grout of series 1, respectively, and 0.19 MPa and 2.26 MPa for the P- and C-based grout of series 2. These values are sensibly lower than the experimental ones. For the bars with P-based grout, the experimental maximum values of τ_u, calculated as average values along S_b and listed in Table 5, are variable in the range 3.6–6.2 MPa for series 1 and in 1.3–2.7 MPa for series 2. Moreover, for the bars with C-based grout, the experimental values of τ_u range in 2.5–3.5 MPa for series 2 and in 4.3–5.9 MPa for series 1.

In Table 7 the theoretical values of pull-out forces given by Eqs. (6)–(10) are listed for both series of tests assuming for f_g the average values of the experimental compressive strength, $f_{g,av}$, as reported in Table 1.

Note that for the bars embedded in the P-based grout, since a bond failure at the bar-grout interface was always observed in both series, only the predictions given by Eqs. (6) and (7) should be used. Conversely, because for the bars embedded in the C-based grout the experimentally observed failure modes were mixed in the tests of both series, i.e. interface bond failures and cone-shaped masonry failure, the theoretical failure loads given by Eqs. (8)–(10) should furnish more reliable previsions. However, for the bars embedded in the C-based grout also the predictions given by Eqs. (6) and (7) have been listed in Table 7 in order to check the possibility of attaining the bar/grout interface failure. Finally in Table 7 the ratios of the theoretical-to-experimental loads, $F_{th}/F_{max,av}$, are also listed for the five strength models considered. Note that the average values of maximum loads do not consider the results of bars with reduced bonded lengths (about 150 mm, see Tables 3 and 4).

4.2.1. Bar-Grout bond interface failure

Both steel and GFRP bars embedded in the P-based grout of both series 1 and 2 attained mainly a B/G interface failure. The low theoretical values of τ_u given by Eq. (11) for the P-based grout determined also the excessively low theoretical loads given by Eq. (6), that, nevertheless is declared valid for a generic 'bond failure', can be reasonably associated to a B/G interface failure, since the bonded bar surface S_b is used. The theoretical loads (5.9 kN for series 1 and 3.6 kN for series 2) are, indeed, significantly lower than the experimental ones in case of B/G interface failure. As previously discussed, (see Section 3.6), these comparisons confirm that the bond strength cannot depends on the only mechanical properties of the grout.

Conversely, the use of Eq. (6) for the bars embedded in the C-based grout gives contrasting results for series 1 and 2: for the series 1, indeed, the theoretical values (77.7 kN) are more than 70% higher than the experimental ones, thus, confirming that the failure mode cannot occur at the bar/grout interface. It is worth to note that such a high estimation of the failure load is related the high compressive strength of the C-based grout of series 1 that influences the value of τ_u used in Eq. (6). For tests of series 2 the theoretical value given by Eq. (6) is 20–25% lower than the experimental ones, but failure did not occur at the bar/grout interface. Again these results are related to the theoretical values of τ_u that are based only on the grout compressive strength.

A more reliable, but however safe, prediction for the bars embedded in the P-based grout is provided by Eq. (7) (Arifpovic and Nielsen, 2006 [34]), which is specific to bar-grout bond failure for anchors completely embedded in masonry units and it is independent on the grout properties. The theoretical loads given by Eq. (7) are 34% and 68% of the average experimental loads for the steel bars of series 1 and 2, respectively, and 43% of the average experimental loads for the GFRP bars of series 1, while are comparable for the GFRP bars of series 2.

Also for the bars embedded in the C-based grout, Eq. (7) furnishes a significant underestimation of the experimental loads, i.e. about 60% and 40% for series 1 and 2, respectively; prediction of B/G interface failure given by Eq. (7) is, thus, too safe, even if, differently from Eq. (6), the grout strength is not taken into account in Eq. (7).

4.2.2. Grout-Masonry bond interface failure – mixed failure

Also the Eq. (8) (CEB, 1994 [39]; ACI 318, 2011 [27], *fib* 58, 2011 [36]) is based on the theoretical value of τ_u calculated by Eq. (11), but in this case the grout-masonry interface is assumed as failure surface. The theoretical values given by Eq. (8) are about 4 times higher than the experimental ones of the bars embedded in the C-based grout for series 1 and about 2 times for series 2. The low reliability of such prediction is again related to the value of τ_u only depending on the grout strength.

Eq. (9) (Cook et al., 1993 [35]) has a more complex expression since it is specific for mixed failure mode and is calculated considering the theoretical values of τ_u given by Eq. (11) and the bar diameter, d_b; despite of the dependence on more parameters, the theoretical values overestimate the results of series 1 of about 30% and underestimate the ones of series 2 by 40% in average.

Table 7
Comparison between experimental and theoretical pull-out forces for bond failure.

Series	Grout	Series	Bar	$F_{max,av}$ [kN]	Theoretical values, F_{th} [kN]					$F_{th}/F_{max,av}$				
					Eq. (6)	Eq. (7)	Eq. (8)	Eq. (9)	Eq. (10)	Eq. (6)	Eq. (7)	Eq. (8)	Eq. (9)	Eq. (10)
1	C	SC	Steel	45.3	77.7	16.1	194.2	57.4	32.2	1.72	0.36	4.29	1.27	0.71
		GC	GFRP	44.5						1.75	0.36	4.36	1.29	0.72
	P	SP	Steel	47.3	5.9		–	–		0.12	0.34	–	–	–
		GP	GFRP	37.3						0.16	0.43	–	–	–
2	C	SC	Steel	57.2	42.6	32.2	106.5	32.9	65.5	0.74	0.56	1.86	0.58	1.15
		GC	GFRP	52.6						0.81	0.61	2.02	0.63	1.25
	P	SP	Steel	47.6	3.6		–	–		0.08	0.68	–	–	–
		GP	GFRP	32.9						0.11	0.98	–	–	–

The differences in experimental loads and theoretical predictions are dampened when Eq. (10) (Arifpovic and Nielsen, 2006 [34]) is used; however, Eq. (10), underestimates the average experimental loads of series 1 of about 30% and overestimates the average experimental loads of series 2 of 20% in average. Note that in Eq. (10) there is no dependence on the grout strength, the parameter l_u is the unit masonry length (200 mm for the case at hand), and the compressive strength of the mortar joints of the masonry texture, f_j, is assumed equal to that of the tuff blocks, as is frequently the case for masonry of this type (Augenti and Parisi, 2010 [40]).

4.3. Reliability of theoretical formulation

The comparisons of experimental and theoretical values of maximum pull-out forces showed that the presented strength models are not all able to reliably catch the experimental results, unless the formulation of (Arifpovic and Nielsen, 2006 [34], i.e. Eq. (10)), which is, however, completely independent of the grout strength. One of the main defect of these formulations is that none of them directly accounts for the surface properties of the bars that surely are a crucial issue for the efficiency of the injected anchors. The surface treatment of the bar certainly influences the shear strength and, in particular, affects the contribution due to the mechanical interlocking along the bar/grout interface, whereas the ramification of the grout within the masonry and, thus, the damage status of the masonry (cracks, voids, etc.) influences the interlocking along the grout-masonry interface.

Moreover, it worth noting that the performances of the injected anchors can be highly variable depending on the type of grout; some of these formulation take into account the effect of the grout only by means of its compressive strength, but the experimental results highlighted that this could not be the only parameter influencing the problem. A different chemical compositions of the grout could lead to different adhesion properties. A very high compressive strength may not necessarily result in beneficial effects on the anchor performance, since intervention effectiveness is limited by the masonry strength and, if the grout strength is also associated to a very high stiffness, an excessive stress transfer in the masonry surrounding the anchor may lead to a premature masonry failure.

Another important issue is the assessment of the shear bond strength; if it is calculated as average values along the embedded length of the anchor, l_e, such a value clearly depends on l_e and on the bonded surface under consideration (bar or borehole). To clarify such an aspect, specific pull-out bond tests should be carried out in order to assess 'local' shear-slip relations basing on 'short' bonded length and aimed to better identify the influence of all the aforementioned parameters.

5. Parametric analysis of out-of-plane mechanisms of a masonry façade

One of the questions still open for the possible application of the injected anchors as strengthening intervention in masonry walls concerns its obtrusiveness, especially for heritage buildings, if the number of anchors needing for avoiding out-of-plane mechanisms becomes high. In order to check the obtrusiveness of such an intervention technique, numerical parametric elaborations have been carried out for investigating the number of anchors needing for avoiding out-of-plane mechanisms, basing on the pull-out forces registered in the experimental tests herein presented. In particular, the parametric analyses were aimed to: 1) assess the range of activation of out-of-plane damage mechanisms in masonry walls under seismic actions, and 2) evaluate the consequent level of horizontal force that should be provided by local connecting systems when the wall equilibrium is not satisfied.

To be specific, a case study represented by a façade panel consisting of tuff masonry and characterized by four storeys equally distributed over the total height of 12 m (i.e., an inter-storey distance of 3 m) was considered. Different thicknesses, t, of the panel were examined (0.6-1.0 m) to simulate slenderness values, $\lambda = H/t$, variable between 12 and 20, which are typical for existing masonry structures. The length of the masonry panel was 6 m and the unit weight of masonry was 14 kN/m^3, which is a typical value for tuff masonry. The four floors had a span length of 5 m and were assumed to be simply supported on the masonry walls, with the resultant force applied at 1/3 of the wall thickness from the external edge. The permanent and variable loads on the floors were estimated to be $g_k = 5.4$ kN/m^2 and $q_k = 2$ kN/m^2, respectively, under the assumptions of a standard floor made of bricks and reinforced concrete elements and of a building intended for residential use. In the calculation, the loads were considered in accordance with the ultimate limit state combination (EN 1992-1-1: 2004, 2004 [44]).

The seismic actions at the base, according to the Italian code provisions, are represented by $a_g{\cdot}S$, where a_g is the peak ground acceleration and S is the topographic amplifying factor; in this example, the seismic action $a_g{\cdot}S$ was computed to range between 0.05g and 0.50g, being g the gravitational acceleration. The acceleration was distributed over the height of the façade in accordance with the following law suggested for the local verification of masonry elements under seismic actions:

$$a_g(z) = \frac{a_g S}{q} \cdot \left[\frac{z}{H} \cdot \frac{3N}{2N+1}\right] \tag{12}$$

where z is the height of the centre of gravity for each panel with respect to the ground level, H is the total height of the structure, q is a behaviour factor that can be assumed equal to 2 for such verifications, and N is the number of floor of the building. It is worth to note that Eq. (12) is a simplified, but safe version of the original formulation suggested in [15], since in Eq. (12) the periods of the whole structure and of the masonry wall subjected to the out-of-plane mechanism have been assumed equal.

The purpose of the analyses was to verify whether the equilibrium was satisfied for the following four out-of-plane storey damage mechanisms (see Fig. 11a):

- Four-storey mechanism: hinge positioned at the base;
- three-storey mechanism: hinge positioned at the first floor;
- two-storey mechanism: hinge positioned at the second floor;
- upper-storey mechanism: hinge positioned at the third floor.

The analyses were performed under the usual assumptions [15] of no tensile strength of the masonry, no slip between the blocks along the mortar joints, i.e. monolithic behaviour of walls, and infinite compressive strength of the masonry; under these hypotheses, the failure mechanism occurs only as a result of a loss of equilibrium of the considered wall and is not related to the masonry strength. In particular, the equilibrium is assured if the total stabilizing moment is greater than the de-stabilizing moment; both moments are calculated with respect to the rotation point of each scheme, as shown in Fig. 11a.

The stabilizing contributions are the vertical loads represented by the weights of the panels, N_j, which are applied at the centre of gravity of each panel, and the loads transferred by the floors, N_{fj}, which are applied at the floor level.

The de-stabilizing contributions are represented by the horizontal forces due to seismic action related to the masses of the panel that is assumed susceptible of out-of-plane rotation, $S_{N,tot}$, and of the related floors, S_{Nfj}. Both forces were computed using Eq. (12) under the assumption that $S_{N,tot}$ was applied at the centre of mass of the panel and S_{Nfj} at the level of the j-th floor.

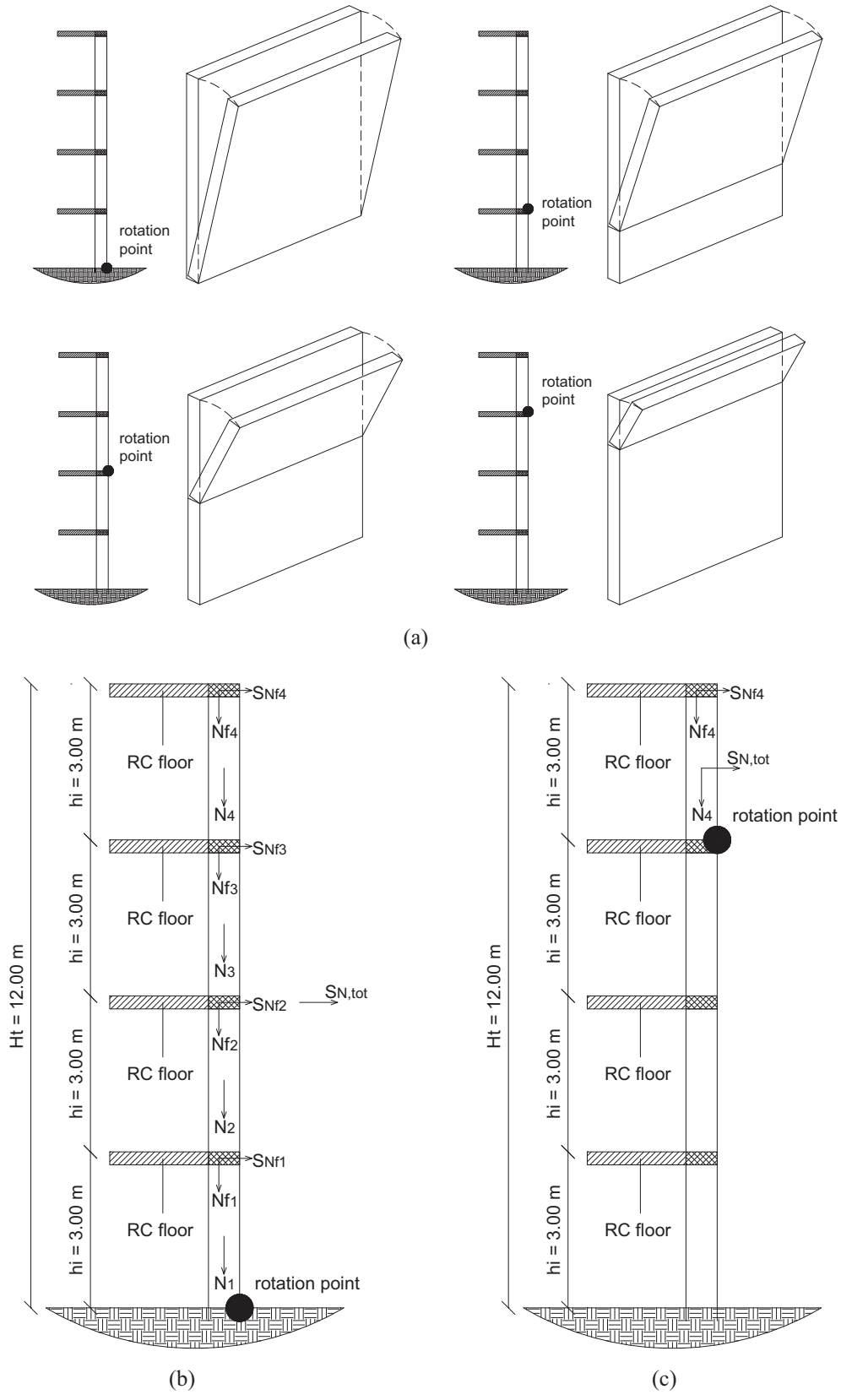

Fig. 11. a) Schematic drawing of out-of-plane mechanisms considered in the parametric analyses; load contributes considered in the equilibrium for the case of rotation point placed (b) at the base and (c) at the third level.

In Fig. 11b and c, examples of the distribution of the acting forces in the cases of rotation point placed at the ground and at the third level are depicted, respectively.

If the equilibrium requirements are not satisfied, then it is possible to determine the extent of the additional horizontal force, F_h, that is needed to compensate for the difference between the stabilizing and de-stabilizing contributions. Such a force F_h is supposed to be adsorbed by a connecting system consisting of 3 injected anchors equally spaced (0.75 m) along both lateral sides of each wall placed above the rotation point, just in order to make the intervention as less invasive as possible. The anchors are considered to be applied parallel to the horizontal action, i.e. orthogonal to the walls susceptible of out-of-plane mechanisms. Fig. 12a and b show the position of the anchors for the case of hinge placed at the ground and at the third level, respectively.

The following linear distribution of forces was considered among the anchors placed in the wall subjected to the out-of-plane mechanism:

$$F_i = M_{sd} \cdot \frac{y_i}{\sum_{i=1}^{n} y_i^2} \tag{13}$$

where F_i is the force on a single anchor, M_{sd} is the amount of non-equilibrated moment that has to be globally absorbed by the connecting system, and y_i is the vertical distance of the i-th anchor from the hinge.

In Figs. 13a–c and 14a, the variation in the maximum horizontal force F_i required to ensure equilibrium in the most highly stressed injected anchor is plotted as a function of $a_g S$ for different values of slenderness, λ, and for the four hinge positions. The average values of the three higher pull-out loads obtained in the experimental tests of series 2 ($F_{max,av}$, Table 4), i.e. the failure loads attained by the steel and GFRP bars embedded in the C-based grout and by the steel bars embedded in the P-based grout, are also plotted in Figs. 13 and 14 for comparison.

When the hinge is placed at the third level, the case in which no vertical load to the wall of the last floor is applied was also considered (Fig. 14b). In this case, the last floor is not subjected to the stabilizing contribution N_{f4}, but only to the de-stabilizing contribution S_{Nf4}, leading, thus, to a less safe situation.

The graphs presented in Figs. 13 and 14 show that the required force clearly increases as the seismic acceleration, $a_g \cdot S$, increases and as the number of floors involved in the mechanism increases; therefore, the maximum force is demanded when the hinge is placed at the ground floor (Fig. 13a). Moreover, it is worth noting that in the worse cases, i.e. hinge located at the ground (Fig. 13a) or first floor (Fig. 13b), for an assigned value of $a_g \cdot S$, the maximum force increases with the wall slenderness, λ, for $a_g \cdot S < 0.15$–0.20 g, whereas the maximum force decreases as λ increases for $a_g \cdot S > 0.15$–0.20 g.

Conversely, when the hinge is placed at the second floor (Fig. 13c) the trend changes respect to the previous cases, since the maximum load increases with the slenderness until $a_g S$ is about 0.4. Moreover, when the hinge is placed at the third floor (Fig. 14a and b), the maximum force always increases with increasing slenderness, regardless of the value of $a_g \cdot S$. These different trends arise because the variation in λ is induced by a variation in the wall thickness, which also gives a variation in the weight upon which depend both the stabilizing (weight of the wall) and de-stabilizing (seismic action related to the weight of the wall) contributions to the global equilibrium. In particular, when the

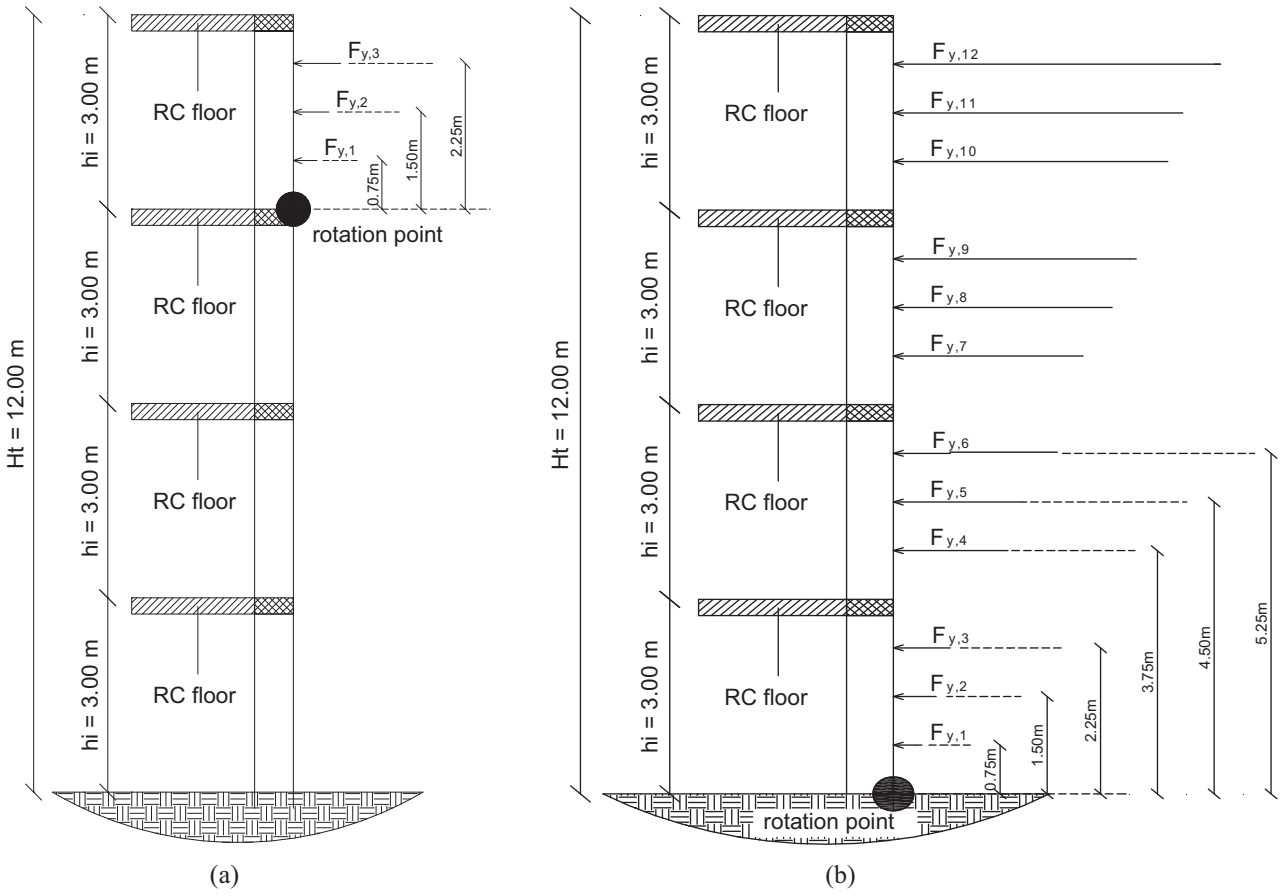

Fig. 12. Example of the linear force distribution in the anchors in the case of rotation point placed at: a) the third level, b) the ground level.

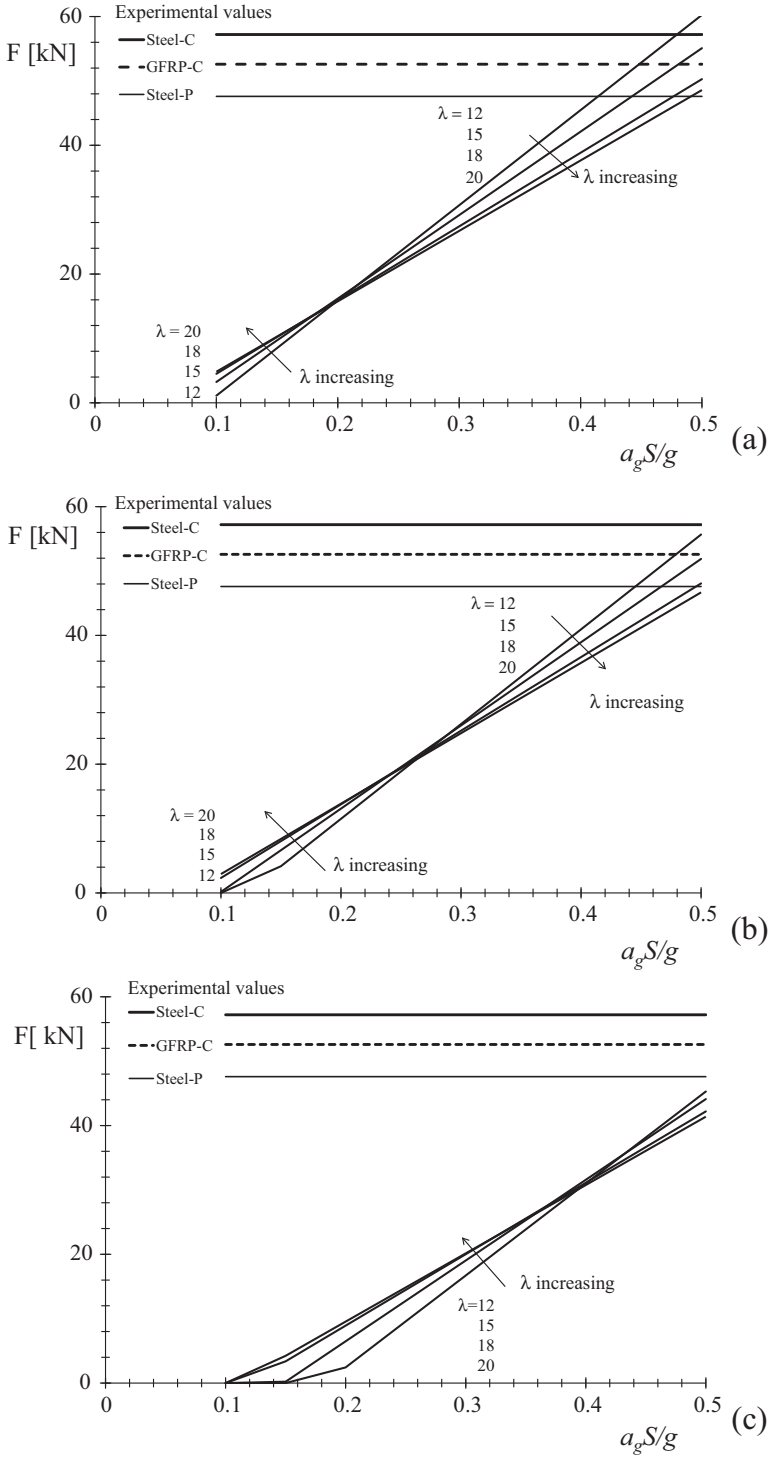

Fig. 13. Maximum force in the most highly stressed anchor vs. $a_g S/g$ for masonry walls with variable slenderness at for different positions of the rotation point: a) at the base; b) at the first floor; c) at the second floor.

hinge is located at the ground or first floor, the proportion of the façade panel that is involved in the mechanism corresponds to 100% or 75% of the entire façade. Therefore, because of the large amount of mass involved, the reduction in the de-stabilizing contribution originating from the seismic action is more beneficial, in terms of equilibrium, than the corresponding reduction in the stabilizing contribution originating from the weight. For this reason, an increase in λ is favourable because it reduces the weight of the wall and, thus, the corresponding seismic action as well.

For the worse cases (hinge at the ground and first floor, i.e. Fig. 13a and b), the experimental average pull-out force for the steel bar embedded in the C-based grout, i.e. the highest experimental value attained in series 2, is higher than the required force for $a_g \cdot S < 0.4$–0.5 g depending on the value of λ. It is worth also to note that the lower experimental loads attained by the steel bars embedded in the P-based grout and the GFRP bars embedded in the C-based grout are higher than the required force for $a_g \cdot S < 0.38$ g and $a_g \cdot S < 0.35$ g, respectively, for whatever value of λ.

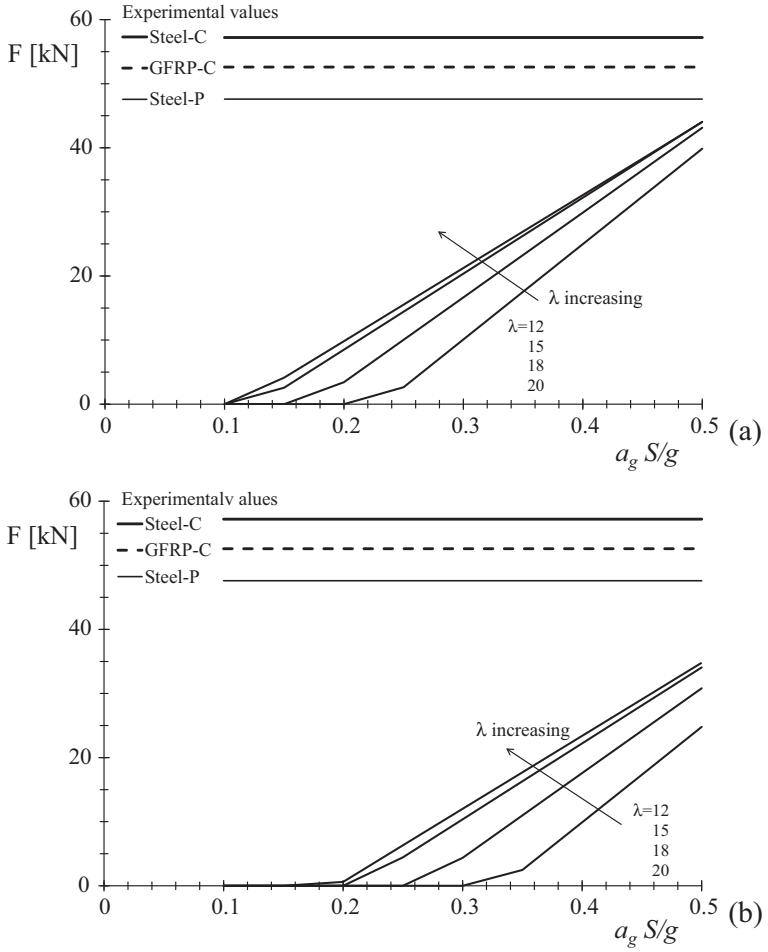

Fig. 14. Maximum force in the most highly stressed anchor vs. $a_g S/g$ for masonry walls with variable slenderness in the case of rotation point at the third floor: a) presence of vertical load N_{f4} on the walls of last floor; b) absence of N_{f4} on the walls of the last floor.

Moreover, when the hinge is located at the second floor (Fig. 13c), the highest experimental failure load is greater than the required force for $a_g \cdot S < 0.42$, independently on λ, while the other two experimental loads are greater than the required force for $a_g \cdot S < 0.4$ and 0.36, respectively.

Finally, when the hinge is located at the third floor (Fig. 14a and b), all the three experimental loads are higher than the required force, regardless of value of $a_g \cdot S$ varying in the range 0–0.5 g.

In conclusion, this simple application highlights that the steel bars embedded both in the C-based and P-based grout and the GFRP bars embedded in the C-based grout tested in the second series of the pull-out tests previously described, appear to be an effective and low invasive technique for preventing out-of-plane mechanisms under medium-high seismic actions.

6. Conclusions

In the first part of the paper the results of experimental in-situ pull-out tests of injected anchors realized in existing masonry walls made of yellow tuff were presented. Two series of pull-out tests have been carried out on deformed steel and GFRP bars with diameter 12 mm (series 1) and 20 mm (series 2) embedded in two types of grout: a cement-based (high strength grout) and a pozzolana-based (low strength) grout. Both grout mix used for series 2 are characterized by lower strength compared with the ones used in series 1. After the detailed discussion of the experimental results, the maximum pull-out forces have been also compared with some literature formulations.

The second part of the paper is devoted to verify the efficiency of the tested anchoring systems for avoiding out-of-plane mechanisms of masonry walls associated with several positions of the rotation point in an example masonry façade (thickness ranging in 0.6–1.0 m, height 12 m, variable slenderness λ = 12–20) subjected to horizontal seismic forces. Such parametric analyses have been carried out assuming the injected anchors equally distributed over the height of the wall subjected to the out-of-plane mechanism (spacing 0.75 m).

The analysis of the experimental results evidenced that:

- the cement-based grout allowed the highest pull-out loads to be attained for both types of bars and led to a partial cone-shaped failure mechanism in the masonry, especially in the case of the steel bars;
- the pozzolana-based grout always exhibited a bar-grout interface failure and attained often worse performance compared with the cement-based one;
- the steel bars have always achieved higher pull-out loads compared with the GFRP bars, which are characterized by twisted glass fibers along their surfaces; such a surface treatment was probably not as effective in activating aggregate interlocking phenomena as are the ribs of the steel bars;
- the use of larger bar diameter in series 2 did not provide proportional load increase for the bars embedded in the cement-based

grout, with consequent lower exploiting rates of the bar tensile strength; conversely, for the bars embedded in the pozzolana-based grout, the bar diameter increase caused in the tests of series 2 maximum loads comparable or even slightly lower than the values attained in series 1. These results are also ascribable to the use of different mix for the cement- and the pozzolana-based grout of series 2 that was characterized by a compressive strength reduction of about 50% for both types of grout. Such a strength reduction was detrimental especially for the bars embedded in the pozzolana-based grout;
- different local bond behaviour have been observed for the two types of grout and of bars tested in series 2, in terms of both chemical adhesion and interlocking phenomena.

Therefore, basing on the experimental results, the following suggestions can be furnished:

- the use of FRP bar as injected anchor systems surely enhances durability of intervention, but special attention has to be paid to the surface roughness of the bars since the bond behaviour may be less efficient, especially in terms of interlocking phenomena, and lead to lower maximum pull-out forces;
- the use of very high strength grout could be not convenient because the strength of the grout may be not fully exploited and, if the high strength is coupled with high stiffness too, detrimental shear stress concentration in the masonry around the anchor may occur. Basing on the experimental outcomes herein presented, the use of grout with compressive strength variable within 20–40 MPa is suggested;
- the use of large diameter should be not convenient compared with the use of similar bars with smaller diameter, since the pull-out load does not increase proportionally. Moreover, it is worth to note that as the bar diameter is smaller as the diameter of the borehole is lower and the strengthening intervention is, thus, less invasive;
- suitable safety factors have to be considered on the assessment of the bonded length in order to take into account the uncertain quality of realization, which depends on chemical, physical and rheological properties of the grout, on the pressure used for injecting the grout, and on the cracking and damage status of the masonry around the borehole. However, longer bonded length are suggested and, in particular, bonded length-to-borehole diameter ratio, l_e/d_g, greater than 10 are suggested (medium anchorage).

The comparisons between the experimental pull-out forces and some literature provisions disclosed that in most cases the predicted values are less reliable mainly because the surface treatment of the bars is not taken into account and the influence of the grout compressive strength on the theoretical value is too strong. To better investigate such an issue and assess the influence of several parameters, more experimental information need about the local values of shear bond strength.

The theoretical tensile forces obtained in the parametric analyses and devoted to avoid the occurrence of out-of-plane damage mechanisms were compared with the three higher experimental pull-out forces obtained in the tests of series 2. The comparison indicated that the most efficient injected anchors (i.e., the steel bars with diameter 20 mm embedded in the cement-based grout) allowed to equilibrate the overturning moment for values of $a_g{\cdot}S$ lower than 0.4–0.5 g, being the range function of the wall slenderness, λ. This latter result confirms that the tested injected anchors are an effective and low invasive technique for preventing out-of-plane mechanisms of masonry walls under medium-high seismic actions.

Acknowledgements

Research activities presented in this paper have been developed within the research project PON PROVACI in collaboration with STRESS scarl.

The Authors would thank ATP srl and Mapei srl for providing the materials (bars and grouts) used in the experimental tests.

References

[1] P.B. Lourenço, N. Mendes, L.F. Ramos, D.V. Oliveira, Analysis of masonry structures without box behavior, Int. J. Arch. Heritage 5 (4–5) (2011) 369–382.
[2] I. Senaldi, G. Magenes, A. Penna, A. Galasco, M. Rota, The effect of stiffened floor and roof diaphragms on the experimental seismic response of a full-scale unreinforced stone masonry building, J. Earthquake Eng. 18 (3) (2014) 407–443. Taylor and Francis.
[3] M. Valluzzi, F. da Porto, E. Garbin, M. Panizza, Out-of-plane behaviour of infill masonry panels strengthened with composite materials, Mater. Struct. 47 (12) (2014) 2131–2145.
[4] E. Hamed, O. Rabinovitch, Out-of-plane behavior of unreinforced masonry walls strengthened with FRP strips, Compos. Sci. Technol. 67 (3–4) (2007) 489–500.
[5] G. Brandonisio, G. Lucibello, E. Mele, A. De Luca, Damage and performance evaluation of masonry churches in the 2009 L'Aquila earthquake, Eng. Fail. Anal. 34 (2013) 693–714.
[6] C. Modena, F. Da Porto, F. Casarin, M. Marco, S. Elena, Cultural heritage buildings and the Abruzzo Earthquake: performance an post-earthquake actions, Adv. Mater. Res. 133–134 (2010) 623–628.
[7] R. Bento, M. Lopes, R. Cardoso, Seismic evaluation of old masonry buildings. Part II: analysis of strengthening solutions for a case study, Eng. Struct. 27 (2005) 2014–2023.
[8] S. Bhattacharya, S. Nayak, S. Dutta, A critical review of retrofitting methods for unreinforced masonry structures, Int. J. Disaster Risk Reduction (2014), http://dx.doi.org/10.1016/j.ijdrr.2013.12.004, 51-67.
[9] ICOMOS – International Council on Monument and sites, Recommendations for the analysis, conservation and Structural restoration of Architectural Heritage, in: Document Approved in the Committee Meeting in Barcelona the 15th June 2005, 2005.
[10] M. Valluzzi, F. da Porto, C. Modena, Behavior and modeling of strengthened three-leaf stone masonry walls, RILEM Mater. Struct. 37 (2004) 184–192.
[11] A. Penna, P. Morandi, M. Rota, C.F. Manzini, F. da Porto, G. Magenes, Performance of masonry buildings during the Emilia 2012 earthquake, Bull. Earthquake Eng. 12 (5) (2013) 2255–2273.
[12] F. Ceroni, A. Prota, Case study: seismic upgrade of a masonry bell tower by GFRP ties, ASCE J. Compos. Constr. 13 (3) (2009) 188–197.
[13] E. Vintzileou, A. Miltiadou-Fezans, Mechanical properties of three-leaf stone masonry grouted with ternary or hydraulic lime-based grouts, Eng. Struct. 30 (2008) 2265–2276.
[14] T. Valente, J. Barros, F. Ceroni, M. Pecce, Influence of embedded through section connectors on the behavior of a new strengthening technique for concrete structures, in: Proc. of CONSEC2016, 12–14 September 2016, Lecco, Italy, 2016.
[15] Circolare 617, Istruzioni per l'applicazione delle "Nuove norme tecniche per le costruzioni" di cui al D.M. 14 gennaio 2008, Ministero dei Lavori Pubblici, Roma, 02/02/2009 (in Italian).
[16] B. Gigla, Bond strength of injection anchors as supplementary reinforcement inside historic masonry, in: Proc. of 13th International Brick and Block Conference, Amsterdam, The Netherlands, 2004, 29 September–2 October 2004, 2004, pp. 19–28.
[17] S. Paganoni, D. D'Ayala, Testing and design procedure for corner connections of masonry heritage buildings strengthened by metallic grouted anchors, Eng. Struct. 70 (2014) 278–293.
[18] C. Algeri, E. Poverello, G. Plizzari, E. Giuriani, Experimental study on the injected anchors behaviour on historical masonry, Adv. Mater. Res. 133–134 (2010) 423–428.
[19] A. Araujo, V. Oliveira, P.B. Lourenco, Experimental behavior of masonry wall-to-timber elements connections strengthened with injection anchors, Eng. Struct. 81 (2014) 98–109.
[20] M. Panizza, P. Girardello, E. Garbin, M.R. Valluzzi, G. Cardani, M. Dalla Benetta, P. Casadei, On-site pull-out tests of steel anchor spikes applied to brickwork masonry, Key Eng. Mater. 624 (2015) 266–274.
[21] J.B. Tubbs, D.G. Pollock, D.I. McLean, Testing of anchor bolts in concrete block masonry, Masonry Soc. J. 18 (2) (2000) 81–92.
[22] A.M. Fabrello-Streufert, D.G. Pollock, D.I. McLean, Anchor bolts in masonry under combined tension and shear loading, Masonry Soc. J. 21 (1) (2003) 13–20.
[23] B. Benmokrane, B. Zhang, A. Chennouf, Tensile properties and pullout behaviour of AFRP and CFRP rods for grouted anchor applications, Constr. Build. Mater. 14 (3) (2000) 157–170.
[24] M. Robert, B. Benmokrane, Combined effects of saline solution and moist concrete on long-term durability of GFRP reinforcing bars, Constr. Build. Mater. 38 (2013) 274–284.

[25] F. Ceroni, E. Cosenza, G. Manfredi, M. Pecce, Durability issues of FRP rebars in reinforced concrete members, Cement Concr. Compos. 28 (10) (2006) 857–868.
[26] MSJC, Masonry Standard Joint Committee's,, Building Code Requirements for Masonry Structures, (TMS 402-13/ACI, 530-13/ASCE), 2013, pp. 125–128.
[27] ACI 318, Building Code Requirements for Structural Concrete (ACI 318-11) and Commentary, 2011.
[28] T.P. Tassios, Properties of bond between concrete and steel under load cycles idealizing seismic actions, Proc. Of AICAP-CEB Symposium, Rome, CEB Bulletin d'Information 131 (1979) 67–122.
[29] NIKER, Guidelines for assessment and improvement of connections in buildings, in: Final Reports D10.2 – New Integrated Knowledge based Approaches to the Protection of Cultural Heritage from Earthquake Induced Risk, NIKER, Contract FP7-ENV-2009-1, n. 244123, 2012.
[30] B. Gigla, F. Wenzel, Design recommendations for injection anchors as supplementary reinforcement of historic masonry, in: Proc. of 12th International Brick/Block Masonry Conference, Madrid, Spain, 25–28 June 2000, 2000, pp. 691–706.
[31] W.M. McGinley, Design of anchor bolts in masonry, Prog. Struct. Mater. Eng. 8 (4) (2006) 155–164.
[32] R. Allen, J.G. Borchelt, R.E. Klingner, R. Zobel, Proposed provisions for design of anchorage to masonry, Masonry Soc. J. 18 (2) (2000) 35–59. The Masonry Society (TMS).
[33] A. Meyer, R. Eligehausen, Injection anchors for use in masonry structures, in: Proc. of 13th International Brick and Block Conference, Amsterdam, The Netherlands, 29 September–2 October 2004, 2004, pp. 109–117.
[34] F. Arifpovic, M.P. Nielsen, Strength of anchors in masonry, Department of Civil Engineering, Technical University of Denmark, Rapport BYG DTU No. R-134, ISSN 1601–2917, ISBN 87-7877-205-2, 2006.
[35] R.A. Cook, G.T. Doerr, R.E. Klingner, Bond stress model for design of adhesive anchors, ACI Struct. J. 90 (5) (1993) 514–524.
[36] fib Bulletin 58, Design of anchorages in concrete: guide to good practice, fédération internationale du béton, Special Activity Group 4, Fastenings to structural concrete and masonry structures, 978-2-88394-098-7, 2011.
[37] R. Eligehausen, R.A. Cook, Behavior and design of adhesive bonded anchors, ACI Struct. J. 103 (6) (2006) 822–831.
[38] Hilti, North American Product Technical Guide – Anchor Fastening Technical Guide, vol. 2, Hilti Inc., Tulsa, OK, 2011, p. 2001.
[39] CEB, Comité Euro-International du Béton, Fastenings to Concrete and Masonry Structures. State-of-the-art Report, Thomas Telford, London, 1994.
[40] N. Augenti, F. Parisi, Constitutive models for tuff masonry under uniaxial compression, J. Mater. Civ. Eng. 22 (11) (2010) 1102–1111.
[41] M. Pecce, G. Manfredi, R. Realfonzo, E. Cosenza, Experimental and analytical evaluation of bond properties of GFRP bars, J. Mater. Civ. Eng. 13 (2001) 282–290.
[42] B. Silva, A.E. Pigouni, M.R. Valluzzi, C. Modena, Calibration of analytical formulations predicting compressive strength in consolidated three-leaf masonry walls, Constr. Build. Mater. 64 (2014) 23–38.
[43] A. Araujo, V. Oliveira, P.B. Lourenco, Numerical study on the performance of improved masonry-to-timber connections in traditional masonry buildings, Eng. Struct. 80 (2014) 501–513.
[44] EN 1992-1-1: 2004, European Committee for Standardization, Eurocode 2 – Design of Concrete Structures, Part 1-1 General Rules and Rules for Buildings, 2004.